

Beyond Near-Field: Far-Field Location Division Multiple Access in Downlink MIMO Systems

Haoyan Liu, Jianjie Cai, Min Yang, and Chengguang Li

Abstract

Exploring channel dimensions has been the driving force behind breakthroughs in successive generations of mobile communication systems. In 5G, space division multiple access (SDMA) leveraging massive MIMO has been crucial in enhancing system capacity through spatial differentiation of users. However, SDMA can only finely distinguish users at adjacent angles in ultra-dense networks by extremely large-scale antenna arrays. For a long time, most research has focused on the angle domain of the space, overlooking the potential of the distance domain. Near-field location division multiple access (LDMA) was proposed based on the beam-focusing effect yielded by near-field spherical propagation model, partitioning channel resources by both angle and distance. To achieve a similar idea in the far-field region, this paper introduces a far-field LDMA scheme for wideband systems based on orthogonal frequency division multiplexing (OFDM). Benefiting from frequency diverse arrays (FDA), it becomes possible to manipulate beams in the distance domain. Combined with OFDM, the inherent cyclic prefix ensures a complete OFDM symbol can be received without losing distance information, while the matched filter of OFDM helps eliminate the time-variance of FDA steering vectors. Theoretical and simulation results show that LDMA can fully exploit the additional degrees of freedom in the distance domain to significantly improve spectral efficiency, especially in narrow sector multiple access (MA) scenarios. Moreover, LDMA can maintain independence between array elements even in single-path channels, making it stand out in MA schemes at millimeter-wave and higher frequency bands.

Index Terms

The authors are with the School of Aerospace Science and Technology, Xidian University, Xi'an 710071, China(email:liuhy@xidian.edu.cn)

Far-filed location division multiple access (LDMA), MIMO-OFDM, Frequency diverse arrays (FDA),
downlink

I. INTRODUCTION

A. Background and Motivation

The three primary application scenarios defined in 5G—enhanced mobile broadband (eMBB), massive machine-type communications (mMTC), and ultra-reliable low-latency communications (URLLC)—will encounter increasing challenges in the next generation of wireless communication networks. In 6G, eMBB is expected to support more demanding applications, such as immersive holographic communications and ultra-high-definition video streaming, necessitating significant advancements in spectral efficiency. Simultaneously, mMTC will expand to accommodate the explosive growth of Internet of Things (IoT) devices in smart living and industrial production. Moreover, URLLC will provide real-time control and coordination capabilities for critical applications requiring stringent latency and reliability, such as autonomous vehicle networks and the full automation of interconnected robots in ultra-dense networks [1]. Multiple access (MA) schemes play a crucial role in enhancing service quality in multi-user scenarios. Therefore, it is imperative for new MA technologies to continuously evolve to meet the demands of 6G scenarios, further enhancing system capacity, increasing connection density, reducing power consumption and costs, and minimizing access delays [2], [3].

In previous generations of mobile communication systems, MA schemes such as time/frequency division multiple access, code division multiple access, and orthogonal frequency division multiple access have been employed to separate users using orthogonal channel resources. The evolution to 4G and 5G systems witnessed the emergence of space division multiple access (SDMA), leveraging massive multiple input multiple output (MIMO) technology [4], [5]. The base station (BS) employs advanced precoding methods to allocate each user equipment (UE) a unique steering vector or beam, thereby enabling spatial differentiation of users [6]–[8]. Despite the presence of inter-user interference, the multiplexing of time-frequency resources has significantly increased system capacity. Furthermore, power domain non-orthogonal multiple access has garnered substantial attention in 5G, demonstrating the potential of transmitting superimposed messages from multiple UEs within the same channel resource block [9]. It is evident that the expansion of channel dimensions has markedly accelerated the evolution of communication systems. Contemporaneous schemes, including rate-splitting multiple access [10], pattern division multiple access [11], and sparse code multiple access [12], have optimized interference management strategies from different information processing perspectives, leading to more effective

utilization of existing channel resources. However, these methods lack further development of the available channel dimensions. Some novel MA strategies for 6G have begun exploring the resource dimensions at the backend of communication systems. For instance, Pradhan et al. have applied finite field extensions to MA [13], and Zhang et al. have proposed mode division multiple access based on semantic domain resources [14].

It is apparent that there is yet another dimension in the spatial domain that has rarely been considered: distance. To our best knowledge, Wu and Dai were the first to develop the channel degrees of freedom (DoFs) in the distance domain and proposed the innovative near-field location division multiple access (LDMA) [15]. For extremely large-scale antenna arrays, the Rayleigh distance extends to several tens of meters, indicating that a significant portion of communications will occur in the near-field region characterized by spherical wave propagation. By utilizing the near-field propagation model, beams can focus signal energy within specific locations of a two-dimensional plane [16]. This capability allows the BS to differentiate UEs effectively based on their angles and distances. The beam's focusing capability progressively diminishes as the distance increases, ultimately degrading into planar waves. Thus, the implementation of near-field LDMA is heavily dependent on large-scale arrays and high-frequency electromagnetic waves to extend the Rayleigh distance. Nonetheless, near-field LDMA has demonstrated significant improvements in spectral efficiency through the exploitation of the distance dimension. Likewise, a new challenge arises: how to focus beams in the far-field?

B. Related Work on Frequency Diverse Array (FDA)

FDA is an evolution of the traditional phased array (PA) by applying slight frequency shifts across the various transmitting elements [17]. This frequency diversity causes phase differences when the waves from distinct elements intersect even in the same direction, which forms interference patterns at specific distances and provides the ability to manipulate beams in the distance domain. The original FDA faces two major challenges. The first challenge stems from linear frequency increased offsets, which produce oscillating "S"-shaped beam pattern in the two-dimensional plane. This limitation can be mitigated by employing logarithmic increased [18], random [19], or optimization-based [20] frequency offsets, thus decoupling angle and distance dimensions to form a dot-shaped beam pattern. The second key issue is time-variance of the FDA, preventing the peak from consistently orienting toward the target location. Many efforts have attempted to overcome this obstacle by designing time-modulated frequency offsets [21] or dynamic transmit weights [22]. However, as elucidated in [23], these approaches are fundamentally flawed. The time-variance is an inherent characteristic resulting from the various frequency offsets in

FDA, making it impossible to generate static beams in the distance-angle domain as achieved by PA. A feasible approach is to use matched filtering at the receiver to eliminate time variance [24], rendering the filtered steering vector time-independent and forming a static two-dimensional beam in the digital domain.

In digital communication systems, the emphasis is on the interference yielded by the steering vector within the equivalent baseband model, rather than on whether the beam can maintain its directionality towards the UEs, which means that the time-variant property of FDA does not pose an impediment to its application in communication systems. [25]–[27] proposed integrated sensing and communication schemes based on FDA through embedding information into frequency increments to minimize the impact of communication functions on sensing performance. Subsequently, some studies have incorporated index modulation into FDA-MIMO systems to enhance communication rates [28], [29]. The most pertinent study by Jian et al. explores FDA-based beamforming to transmit secrecy information from the BS to downlink UEs [30]. The consideration of signal propagation delay in FDA leads to the degradation of orthogonality in the matched filter when integrating over the symbol time. In narrowband communication systems, where the propagation delay is much shorter than the symbol time, orthogonality can be approximately maintained, as many studies have neglected this issue [27], [28], [30]. However, the propagation delay will span several tens of symbols in wideband systems. Therefore, to support FDA-based LDMA in high-rate communication scenarios, it is necessary to adopt waveforms that can accommodate propagation delays.

C. Our Contributions

In this paper, we design a far-field LDMA multiple access scheme for the downlink by exploiting the distance resolution capability of FDA in wideband systems. Compared to SDMA, the proposed scheme can effectively mitigate interference between UEs in nearby directions by fully exploring the additional DoFs in the distance domain, thereby enhancing overall system performance. However, the frequency offsets not only result in additional spectral overhead but also yield inter-carrier interferences (ICIs) at the receiver. Furthermore, constrained by the array dimensions, the steering vectors of FDA inevitably exhibit some correlation. Therefore, whether LDMA offers a spectral efficiency improvement over SDMA remains to be further investigated. The main contributions can be summarized as follows:

- Inspired by the FDA technique, the development of far-field LDMA is explored for wideband systems. The key idea is that the inherent cyclic prefix (CP) of orthogonal frequency division multiplexing (OFDM) allows the receiver to maintain excellent subcarrier orthogonality even in the presence of symbol time offset (STO), which provides natural compatibility for the application

of LDMA in practical systems. Moreover, the matched filtering module of the OFDM receiver can simultaneously eliminate the time-variance of the steering vectors and demodulate the information symbols carried by subcarriers. These advantages ensure that the proposed MA scheme does not require any modifications to the receivers on the UE side. Our analysis indicates that the proposed waveform can fully meet the coverage requirements of cellular communication systems.

- We designed frequency offsets with random permutations. The proposed frequency offsets effectively decouple the distance-angle dependency while exhibiting discrete Fourier transform properties in the distance domain, similar to those in the angular domain. We further demonstrated the asymptotic orthogonality of the designed steering vectors and provided the expectation of beam correlation. subsequently, two technical approaches for eliminating ICIs are discussed. Using slight frequency offsets can approximately maintain subcarrier orthogonality without increasing complexity, however, the resulting beamwidth exceeds the maximum propagation distance that the designed waveform can accommodate. In contrast, although the pre-equalization method increases complexity to some extent, it imposes no limitations on maximum frequency offset. This allows for the design of narrower distance-domain beams, enhancing the BS's ability to resolve UEs at different locations.
- The upper bound of LDMA performance has been demonstrated. When the number of UEs is small, such as only two, its performance typically does not surpass that of SDMA. However, as the number of UEs increases, LDMA achieves significant improvements in spectral efficiency by trading off a portion of spectral resources. Simulation results indicate that LDMA can achieve up to a 75% performance improvement when the sector angle is large; for small sector angles, LDMA's spectral efficiency is several times that of SDMA. Therefore, LDMA demonstrates unparalleled advantages in narrow sector multi-user communication scenarios. Mathematical derivation further elucidates the reasons behind the substantial gains of far-field LDMA: traditional SDMA requires a rich scattering environment to ensure strong independence between array elements [31], whereas LDMA can achieve mutual independence even in single-path channels. Thus, LDMA can provide full MIMO channel DoFs without relying on multipath effects for millimeter-wave and future higher-frequency communication systems.

The remainder of the paper is organized as follows. Section II introduces the far-field LDMA system model and provides the equivalent vectorization form. In Section III, the design of random permutation frequency offsets is proposed and the asymptotic orthogonality is proved. Meanwhile, the slight frequency offsets and pre-equalization methods are also discussed. The performance analysis of LDMA is demon-

strated in Section IV. Simulation results are provided in Section VI, and conclusions are drawn in Section VII.

II. SYSTEM MODEL

We consider a wideband time division duplexing (TDD) single-cell MU-MIMO communication system consisting of one BS equipped with M antennas. The BS simultaneously provides services to K UEs, each with N antennas. The transmitter modules of both the BS and the UEs employ the FDA architecture. The channel between the BS and each UE is composed of $P + 1$ propagation paths, comprising one Line-of-Sight (LoS) path and P Non-Line-of-Sight (NLoS) paths. For simplicity in analysis, we assume that the MU-MIMO channel matrix adheres to the block fading condition, which implies that the complex-valued gains associated with each path remain constant throughout a data transmission block. Meanwhile, the Doppler shifts can be perfectly compensated at the receiving end. Furthermore, strict system synchronization is maintained across all devices within the cellular network, and the locations for BS and UEs are known to each other.

A. FDA-MIMO-OFDM transceiver model

We begin by introducing the single-user MIMO-OFDM channel model utilizing the FDA technique in the downlink system. In the TDD system, the uplink physical channel is identical to the downlink channel. Therefore, a similar derivation can be performed for the transmission model from UEs to the BS, which is omitted in this paper. Let $\mathbf{x}_m = [x_{1,m}, x_{2,m}, \dots, x_{N_{\text{us}},m}]^T$ be the information symbols sent by the BS on the m -th antenna. By employing OFDM modulation, the transmit signal of the BS can be expressed as

$$x_m(t) = \sum_{\ell=0}^{N_{\text{us}}-1} x_{\ell,m} g(t) \exp \{j2\pi\ell\Delta f t\}, \quad -T_{\text{cp}} \leq t < T_{\text{us}}, \quad (1)$$

where Δf is the subcarrier spacing, N_{us} is the total number of subcarriers and $g(t)$ is the prototype pulse function. Then, the OFDM symbol duration is $T_{\text{us}} = 1/\Delta f$, and the downlink OFDM signal bandwidth is $B = N_{\text{us}}\Delta f$. Denote N_{cp} as the number of CPs, the CP length is equal to $T_{\text{cp}} = N_{\text{cp}}T_{\text{us}}/N_{\text{us}}$. Suppose that the $g(t)$ has unit energy and satisfies the following orthogonality

$$\int g(t)g^*(t) \exp \{j2\pi(\ell - \ell')\Delta f t\} dt = \delta(\ell - \ell'). \quad (2)$$

Consider a generalized configuration for uniformly-spaced linear FDA made of M antennas. Denote by δf_m the frequency offset of the m -th antenna. Using a ray-tracing based channel modeling approach,

the overall signal arriving at n -th receiving antenna of the k -th UE can be given by

$$y_{k,n}(t) = \frac{1}{\sqrt{MN}} \sum_{m=0}^{M-1} \sum_{p=0}^P \sum_{\ell=0}^{N_{\text{us}}-1} h_p x_{\ell,m} g \left(t - \frac{R_{k,p,m,n}}{c} \right) \exp \left\{ j2\pi(f_c + \ell\Delta f + \delta f_m) \left(t - \frac{R_{k,p,m,n}}{c} \right) \right\}, \quad (3)$$

where f_c is center carrier frequency and the h_p is the p -th the gain associated with the p -th propagation path. Concurrently, $R_{k,p,m,n}$ represents the propagation distance from the m -th transmitting antenna to the n -th antenna at the receiving antenna along the p -th path. c is the speed of light. Here, the noise is omitted for brevity. Assuming both the scatterers and UEs are situated in the far-field regions, the $R_{k,p,m,n}$ can be calculated utilizing the planar-wave propagation model as follows

$$R_{k,p,m,n} = R_{k,p} - (m-1)d \sin \theta_{k,p} - (n-1)d \sin \phi_{k,p}. \quad (4)$$

Taking the first element as the reference element, $R_{k,p}$ represents the distance between the transmit reference element and the receive reference element for the p -th path. Alternatively, $R_{k,p} = R_k + r_{k,p}$, where $r_{k,p}$ denotes the additional path length for the p -th NLoS path relative to the LoS path. The spacing between both the transmitting antennas and receiving antennas is half the wavelength of the center carrier frequency, specifically $d = c/2f_c$. $\theta_{k,p}$ and $\phi_{k,p}$ respectively represent the angle-of-departure (AoD) and angle-of-arrival (AOA) in the p -th path. By Substituting (4) into (3) and making some manipulations, the received signal can be expressed as

$$y_{k,n}(t) = \frac{1}{\sqrt{MN}} \sum_{m=0}^{M-1} \sum_{p=0}^P \sum_{\ell=0}^{N_{\text{us}}-1} \tilde{h}_{k,p} x_{\ell,m} g \left(t - \frac{R_{k,p,m,n}}{c} \right) \exp \left\{ j2\pi(\ell\Delta f + \delta f_m) \left(t - \frac{R_k + r_{k,p}}{c} \right) \right\} \\ \times \exp \left\{ j2\pi(f_c + \ell\Delta f + \delta f_m) \frac{(m-1)d \sin \theta_{k,p} + (n-1)d \sin \phi_{k,p}}{c} \right\} \exp \{ j2\pi f_c t \}. \quad (5)$$

In (5), $\tilde{h}_{k,p} = h_p \exp \{ j2\pi f_c R_{k,p}/c \}$ is the complex gain for the p -th path. The center carrier $\exp \{ j2\pi f_c t \}$ can be removed by performing the down-converted operator. In this paper, we set $f_c \gg N_{\text{us}}\Delta f + \delta f_{M-1}$, a condition that can be satisfied in the majority of communication systems. By this means, we have [21]

$$\exp \left\{ j2\pi(f_c + \ell\Delta f + \delta f_m) \frac{(m-1)d \sin \theta_{k,p} + (n-1)d \sin \phi_{k,p}}{c} \right\} \\ \approx \exp \left\{ \frac{(m-1) \sin \theta_{k,p} + (n-1) \sin \phi_{k,p}}{2} \right\}. \quad (6)$$

At the same time, this setting makes it possible to suppose that all signals from the transmitting antennas arrive at each receiving antenna simultaneously, i.e., $R_{k,p,m,n} \approx R_{k,p}$. With the above approximations,

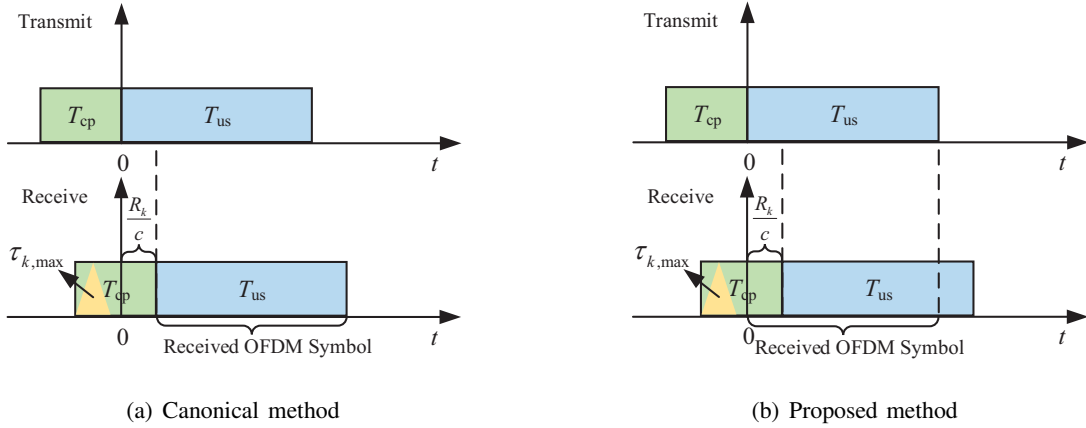


Fig. 1. Illustration of the CP removal method in our designed system.

(5) can be further simplified as

$$\begin{aligned} \bar{y}_{k,n}(t) \approx & \sum_{m=0}^{M-1} \sum_{p=0}^P \sum_{\ell=0}^{N_{us}-1} \tilde{h}_{k,p} \exp \left\{ -j2\pi \ell \Delta f \frac{R_{k,p}}{c} \right\} \mathbf{x}_{\ell,m} \mathbf{a}_m(R_{k,p}, \theta_{k,p}) \mathbf{b}_n(\phi_{k,p}) \\ & \times g \left(t - \frac{R_{k,p}}{c} \right) \exp \{ j2\pi (\ell \Delta f + \delta f_m) t \}, \end{aligned} \quad (7)$$

where $\mathbf{a}(R_{k,p}, \theta_{k,p})$ represents the normalized FDA steering vector at the transmitter

$$\begin{aligned} & \mathbf{a}(R_{k,p}, \theta_{k,p}) \\ & = \frac{1}{\sqrt{M}} \left[1, \exp \left\{ j2\pi \left(\frac{\sin \theta_{k,p}}{2} - \delta f_1 \frac{R_{k,p}}{c} \right) \right\}, \dots, \exp \left\{ j2\pi \left(\frac{(M-1) \sin \theta_{k,p}}{2} - \delta f_{M-1} \frac{R_{k,p}}{c} \right) \right\} \right]^T. \end{aligned} \quad (8)$$

From the above result, it becomes evident that the introduced series of frequency offsets in the spatial domain equips the array with distance-sensing capabilities. Therefore, UEs at different locations can be distinguished by combining angle and distance coordinates.

Similarly, $\mathbf{b}(\phi_{k,p})$ represents the normalized PA steering vector at the receiver

$$\mathbf{b}(\phi_{k,p}) = \frac{1}{\sqrt{N}} \left[1, \exp \left\{ j2\pi \left(\frac{\sin \phi_{k,p}}{2} \right) \right\}, \dots, \exp \left\{ j2\pi \left(\frac{(N-1) \sin \phi_{k,p}}{2} \right) \right\} \right]^T. \quad (9)$$

Unlike the canonical method, the entire CP is discarded directly and the remaining signal is used for OFDM demodulation. To retain distance information in the received signal, our designed receiver preserves signals within the interval $[0, T_{us})$ under strict clock synchronization. Compared to existing FDA methods for handling propagation delay, this approach guarantees the integrality of all symbols. Consequently, a portion of the CP will be utilized in the subsequent signal processing, as shown in Fig. 1. Alternatively, this process can be seen as the intentional introduction of STO. Therefore, it requires

that the CP length should be greater than the maximum propagation delay of the channel, i.e. $T_{cp} \geq R_{k,p}$, rather than the maximum multipath delay spread. Taking 15 kHz subcarrier as an example, the use of 1/4 length CP could accommodate a maximum propagation path of 5 km, which is sufficient to meet the requirements of cellular communication. To retrieve the multiplexed symbols on each subcarrier, a key step is to employ N_{us} corresponding matched filters at the receiver. Considering $g(t)$ as a rectangular pulse, the received symbol on the ℓ' -th subcarrier can be expressed as¹

$$\begin{aligned}
y_{k,\ell',n} &= \int_0^{T_{us}} \bar{y}_{k,n}(t) g^*(t) \exp\{-j2\pi\ell' \Delta f t\} dt \\
&\stackrel{(a)}{\approx} \underbrace{\sum_{m=0}^{M-1} \sum_{\ell=0}^{N_{us}-1} \sum_{p=0}^P \tilde{h}_{k,p} \exp\left\{-j2\pi\ell \Delta f \frac{R_{k,p}}{c}\right\} \mathbf{a}_m(R_{k,p}, \theta_{k,p}) \mathbf{b}_n(\phi_{k,p}) \mathbf{x}_{\ell,m}}_{\mathbf{h}_{k,m,n,\ell}} \\
&\quad \times \frac{1}{N_{us}} \sum_{i=0}^{N_{us}-1} \exp\left\{-j2\pi(\ell - \ell' + \rho_m) \frac{i}{N_{us}}\right\} \\
&= \sum_{m=0}^{M-1} \alpha_m \mathbf{h}_{k,m,\ell' \mathbf{x}_{\ell',m}} + \sum_{m=0}^{M-1} \sum_{\ell=0, \ell \neq \ell'}^{N_{us}-1} \beta_{\ell,\ell',m} \mathbf{h}_{k,m,n,\ell \mathbf{x}_{\ell,m}},
\end{aligned} \tag{10}$$

where approximation (a) is obtained by replacing summation with integral after sampling at intervals of T_{us}/N_{us} , $\mathbf{h}_{k,m,n,\ell}$ can be interpreted as the selective fading generated by multipath channels in both the spatial and frequency domains and ρ_m represents the ratio of frequency offset δf_m to subcarrier spacing.

The coefficients α_m and $\beta_{\ell,\ell',m}$ are given by

$$\alpha_m = \text{Sa}_{N_{us}} \left(\frac{\rho_m}{N_{us}} \right) \exp \left\{ j\pi \rho_m \frac{N_{us} - 1}{N_{us}} \right\}, \tag{11a}$$

$$\beta_{\ell,\ell',m} = \text{Sa}_{N_{us}} \left(\frac{\ell - \ell' + \rho_m}{N_{us}} \right) \exp \left\{ j\pi (\ell - \ell' + \rho_m) \frac{N_{us} - 1}{N_{us}} \right\}, \tag{11b}$$

where the function $\text{Sa}_N(x)$ is defined as

$$\text{Sa}_N(x) = \frac{\sin \pi N x}{N \sin \pi x}. \tag{12}$$

From (10), it can be observed that the frequency offsets on each antenna disrupt the orthogonality of the OFDM subcarriers, leading to ICIs at the receiver. When $\delta f_m = 0, \forall m = 0, 1, \dots, M - 1$, all ICI terms will vanish, and the model degenerates to

$$y_{k,n,\ell} = \frac{1}{N_{us}} \sum_{m=0}^{M-1} \sum_{p=0}^P \tilde{h}_{k,p} \exp \left\{ -j2\pi\ell \Delta f \frac{R_{k,p}}{c} \right\} \mathbf{a}_m(\theta_{k,p}) \mathbf{b}_n(\phi_{k,p}) \mathbf{x}_{\ell,m}, \tag{13}$$

which depicts a traditional MIMO-OFDM system relying on PA transceivers.

¹Distinguishing from existing FDA systems, where matched filters are typically designed as $g(t) \exp\{j2\pi\delta f_m t\}$ to mitigate the time-variance of beam pattern. Here, we select $g(t) \exp\{j2\pi\ell' \Delta f t\}$ as the matched filter signal for OFDM demodulation.

B. Equivalent Vectorization Form

Since the MIMO system can be more compactly represented in vectorization form, the transmitted and received symbols are taken as column vectors for the convenience of the following analysis. Because of the intrinsic ICI yielded in the FDA-MIMO-OFDM system, it is necessary to consider the input-output relationship of all information symbols within an OFDM symbol duration.

Let us define $\mathbf{x} \in \mathbb{C}^{N_{\text{us}}M \times 1}$ as the vectorization form of $x_{\ell,m}$, where its $(mN_{\text{us}} + \ell)$ -th entry is $x_{\ell,m}$, and $\mathbf{y}_k \in \mathbb{C}^{N_{\text{us}}N \times 1}$ as the vectorization form of $y_{k,\ell',n}$, where its $(nN_{\text{us}} + \ell')$ -th entry is $y_{k,\ell',m}$. Based on the system introduced above, an equivalent form of the FDA-MIMO-OFDM transceiver model is given as follows

$$\mathbf{y}_k = \sum_{p=0}^P (\mathbf{I}_N \otimes \mathbf{F}_{N_{\text{us}}}) \mathbf{H}_{k,p} (\mathbf{I}_M \otimes \mathbf{F}_{N_{\text{us}}}^H) (\mathbf{I}_M \otimes \mathbf{\Phi}) \mathbf{x}, \quad (14)$$

where $\mathbf{F}_{N_{\text{us}}}$ denotes the N_{us} -point discrete-Fourier-transform matrix, \otimes denotes Kronecker product, $\mathbf{\Phi}(R_{k,p}) = \text{diag}(1, \exp\{-j2\pi\Delta f R_{k,p}/c\}, \dots, \exp\{-j2\pi(N_{\text{us}} - 1)\Delta f R_{k,p}/c\})$ is the phase shifts caused by the propagation delay on each subcarrier, and $\mathbf{H}_{k,p} \in \mathbb{C}^{N_{\text{us}}N \times N_{\text{us}}M}$ is the space-time domain channel matrix including the effect of M frequency offsets for the p -th path, which can be written as

$$\mathbf{H}_{k,p} = \tilde{h}_{k,p} [\mathbf{b}(\phi_{k,p}) \mathbf{a}^T(R_{k,p}, \theta_{k,p}) \otimes \mathbf{I}_{N_{\text{us}}}] \mathbf{\Xi}. \quad (15)$$

The entries in $\mathbf{\Xi} = \text{diag}(\mathbf{\Xi}_0, \mathbf{\Xi}_1, \dots, \mathbf{\Xi}_{M-1})$ represent the phase shifts caused by frequency offsets at each sampling instant, where $\mathbf{\Xi}_m = \text{diag}(1, \exp\{j2\pi\rho_m/N_{\text{us}}\}, \dots, \exp\{j2\pi\rho_m(N_{\text{us}} - 1)/N_{\text{us}}\})$. By using the Kronecker product rule, the space-frequency domain channel matrix for the vectorized channel input \mathbf{x} and output \mathbf{y}_k for the k -th UE can be obtained by

$$\begin{aligned} \bar{\mathbf{H}}_k &= \sum_{p=0}^P \tilde{h}_{k,p} (\mathbf{I}_N \otimes \mathbf{F}_{N_{\text{us}}}) [\mathbf{b}(\phi_{k,p}) \mathbf{a}^T(R_{k,p}, \theta_{k,p}) \otimes \mathbf{I}_{N_{\text{us}}}] \mathbf{\Xi} (\mathbf{I}_M \otimes \mathbf{F}_{N_{\text{us}}}^H) (\mathbf{I}_M \otimes \mathbf{\Phi}) \\ &= \sum_{p=0}^P \tilde{h}_{k,p} \underbrace{[\mathbf{b}(\phi_{k,p}) \mathbf{a}^T(R_{k,p}, \theta_{k,p}) \otimes \mathbf{F}_{N_{\text{us}}}] \mathbf{\Xi} (\mathbf{I}_M \otimes \mathbf{F}_{N_{\text{us}}}^H) \mathbf{\Phi}}_{\bar{\mathbf{H}}_{k,p}}, \end{aligned} \quad (16)$$

where $\bar{\mathbf{H}}_{k,p}$ is the space-frequency domain channel matrix of the p -path, which can be further explicitly given by the following

$$\bar{\mathbf{H}}_{k,p} = \begin{bmatrix} b_0 a_0 \mathbf{F}_{N_{\text{us}}} \mathbf{\Xi}_0 \mathbf{F}_{N_{\text{us}}}^H \mathbf{\Phi} & b_0 a_1 \mathbf{F}_{N_{\text{us}}} \mathbf{\Xi}_1 \mathbf{F}_{N_{\text{us}}}^H \mathbf{\Phi} & \cdots & b_0 a_{M-1} \mathbf{F}_{N_{\text{us}}} \mathbf{\Xi}_{M-1} \mathbf{F}_{N_{\text{us}}}^H \mathbf{\Phi} \\ b_1 a_0 \mathbf{F}_{N_{\text{us}}} \mathbf{\Xi}_0 \mathbf{F}_{N_{\text{us}}}^H \mathbf{\Phi} & b_1 a_1 \mathbf{F}_{N_{\text{us}}} \mathbf{\Xi}_1 \mathbf{F}_{N_{\text{us}}}^H \mathbf{\Phi} & \cdots & b_1 a_{M-1} \mathbf{F}_{N_{\text{us}}} \mathbf{\Xi}_{M-1} \mathbf{F}_{N_{\text{us}}}^H \mathbf{\Phi} \\ \vdots & \vdots & \ddots & \vdots \\ b_{N-1} a_0 \mathbf{F}_{N_{\text{us}}} \mathbf{\Xi}_0 \mathbf{F}_{N_{\text{us}}}^H \mathbf{\Phi} & b_{N-1} a_1 \mathbf{F}_{N_{\text{us}}} \mathbf{\Xi}_1 \mathbf{F}_{N_{\text{us}}}^H \mathbf{\Phi} & \cdots & b_{N-1} a_{M-1} \mathbf{F}_{N_{\text{us}}} \mathbf{\Xi}_{M-1} \mathbf{F}_{N_{\text{us}}}^H \mathbf{\Phi} \end{bmatrix}, \quad (17)$$

where a_m and b_m represent the m -th and n -th elements in $\mathbf{a}(R_{k,p}, \theta_{k,p})$ and $\mathbf{b}(\phi_{k,p})$, respectively.

Analogously, let $\delta f_m = 0, \forall m = 0, 1, \dots, M-1$, the matrix Ξ_m will degenerate to $\mathbf{I}_{N_{\text{us}}}$, and the $\bar{\mathbf{H}}_{k,p}$ will evolve into a block diagonal matrix. Consequently, the FDA transceiver model is reduced to the following PA transceiver model

$$\mathbf{y}_{k,\ell} = \sum_{p=0}^P \tilde{h}_{k,p} \mathbf{b}(\phi_{k,p}) \mathbf{a}^T(\theta_{k,p}) \exp \left\{ -j2\pi\ell\Delta f \frac{R_{k,p}}{c} \right\} \mathbf{x}_\ell, \quad (18)$$

where $\mathbf{y}_{k,\ell} \in \mathbb{C}^{N \times 1}$, $\mathbf{x}_\ell \in \mathbb{C}^{M \times 1}$ represent the received and transmitted vectors on the ℓ -th OFDM subcarrier. The effective vectorized input-output relationship will be utilized in the MU-MIMO model and subsequent system performance analysis.

C. MU-MIMO Model

Consider a downlink MU-MIMO system, $\mathbf{s} = [(\mathbf{s}_0)^T, (\mathbf{s}_1)^T, \dots, (\mathbf{s}_{K-1})^T]^T$ is the overall information vector, where $\mathbf{s}_k = [s_{k,0}, s_{k,1}, \dots, s_{k,N_{\text{us}}-1}]^T$ is the quadrature amplitude modulation (QAM) symbol vector sent to k -th UE, satisfying $\mathbf{E}[|s_{k,\ell}|^2] = 1$. Then, the transmit signal is given by $\mathbf{x} = \mathbf{W}\mathbf{A}\mathbf{s}$, where $\mathbf{A} = \text{diag}(a_0 \mathbf{I}_{N_{\text{us}}}, a_1 \mathbf{I}_{N_{\text{us}}}, \dots, a_{K-1} \mathbf{I}_{N_{\text{us}}})$ is the power normalisation matrix, a_k is the transmit power allocated to k -th UE. The transmit precoding matrix \mathbf{W} has been extended to $N_{\text{us}}M \times N_{\text{us}}K$ dimension in the FDA system, given by $\mathbf{W} = [\mathbf{W}_0, \mathbf{W}_1, \dots, \mathbf{W}_{K-1}]$. Concretely, $\mathbf{W}_k = \mathbf{w}_k \otimes \mathbf{I}_{N_{\text{us}}}$, where $\mathbf{w}_k \in \mathbb{C}^{M \times 1}$ is the normalized transmit precoding vector of k -th UE satisfying $\|\mathbf{w}_k\|^2 = 1$. The composite channel matrix is given by stacking the space-frequency domain channel matrices on top of each other, given by $\bar{\mathbf{H}} = [\bar{\mathbf{H}}_0, \bar{\mathbf{H}}_1, \dots, \bar{\mathbf{H}}_{K-1}]^T \in \mathbb{C}^{N_{\text{us}}NK \times N_{\text{us}}M}$. The additive noise $\mathbf{n}_k \in \mathbb{C}^{N_{\text{us}}N \times 1}$ follows an independent complex Gaussian variable with zero mean and equal variance σ_n^2 for all users, i.e., $\mathbf{n}_k \sim \mathcal{CN}(\mathbf{0}, \sigma_n^2 \mathbf{I}_{N_{\text{us}}N})$. The received signal at k -th can be written as

$$\mathbf{y}_k = \bar{\mathbf{H}}_k \mathbf{W}_k a_k \mathbf{s}_k + \bar{\mathbf{H}}_k \sum_{i \neq k} \mathbf{W}_i a_i \mathbf{s}_i + \mathbf{n}_k, \quad (19)$$

and the received signal for all K UEs can be represented as

$$\mathbf{y} = \bar{\mathbf{H}}\mathbf{W}\mathbf{A}\mathbf{s} + \mathbf{n}, \quad (20)$$

where $\mathbf{n} \in \mathbb{C}^{N_{\text{us}}NK \times 1}$ is the stacked Gaussian noise vector.

Since the FDA exclusively alters the steering vectors of the transmitting end, the BS can only distinguish UEs based on the direction of signal arrival. Even when UEs employ FDA for transmission, the signals from different antennas are superimposed at the receiving end, preventing the effective matched filtering

of the transmitted steering vectors. Consequently, the LDMA scheme cannot be impractical on the uplink transmission.

III. WAVEFORM DESIGN

From the results in the previous section, it can be observed that frequency offsets endow the perception of distance dimension to the steering vector while disrupting the orthogonality of the OFDM transmission system. Additionally, frequency offsets also determine the orthogonality of the beams in the distance-angle plane. To enhance orthogonal transmission in communication systems, we investigate waveform design schemes based on random permutation frequency offsets in this section. By analyzing the correlation between different steering vectors, the asymptotic orthogonality in distance and angle domain is revealed. Subsequently, we discuss design approaches for orthogonal transmission LDMA systems from two perspectives: employing slight frequency offsets or pre-equalization.

A. Random Permutation Frequency Offsets

In the original FDA, frequency offsets are uniformly increased, i.e., $\delta f_m = (m - 1)\delta f$, where δf is the basic frequency increment cell. Based on the FDA steering vector in (7), the correlation of two beam vectors corresponding to the location of (R_i, θ_i) and (R_j, θ_j) can be formulated as

$$\begin{aligned} |\mathbf{a}^H(R_i, \theta_i) \mathbf{a}(R_j, \theta_j)| &= \frac{1}{M} \left| \sum_{m=0}^{M-1} \exp \left\{ j2\pi m \left(\frac{\sin \theta_i - \sin \theta_j}{2} - \delta f \frac{R_i - R_j}{c} \right) \right\} \right| \\ &= \text{Sa}_M \left(\frac{\sin \theta_i - \sin \theta_j}{2} - \delta f \frac{R_i - R_j}{c} \right), \end{aligned} \quad (21)$$

From (21), the correlation of the steering vectors will achieve the maximum when $(\sin \theta_i - \sin \theta_j) / 2 - \delta f (R_i - R_j) / c = l, l \in \mathbb{Z}$. It can be observed that the distance and angle within the peak region exhibit a sinusoidal relationship, resulting in an "S"-shaped beam pattern as shown in Fig. 2(b). The challenge posed by this "S"-shaped beam lies in the mutual coupling between distance and angle, suggesting that there can be multiple paired solutions for the distance and angle of the target. This ambiguity prevents the beam from precisely focusing on a specific UE. If two LoS path UEs are located within the "S"-shaped beam region, they will experience the same channel, and the BS cannot distinguish between them in the spatial domain.

To generate dot-shaped beams, we first explain the reason for the coupling between distance and angle dimensions. Observing (21), the correlation can achieve the maximum only when the phases of all summation terms are identical, so $\sin \theta_i - \sin \theta_j$ and $R_i - R_j$ need to satisfy the following equation

$$[\mathbf{G}_1, \mathbf{G}_2] [\sin \theta_i - \sin \theta_j, R_i - R_j]^T = [0, l_1, \dots, l_{M-1}]^T, \quad (22)$$

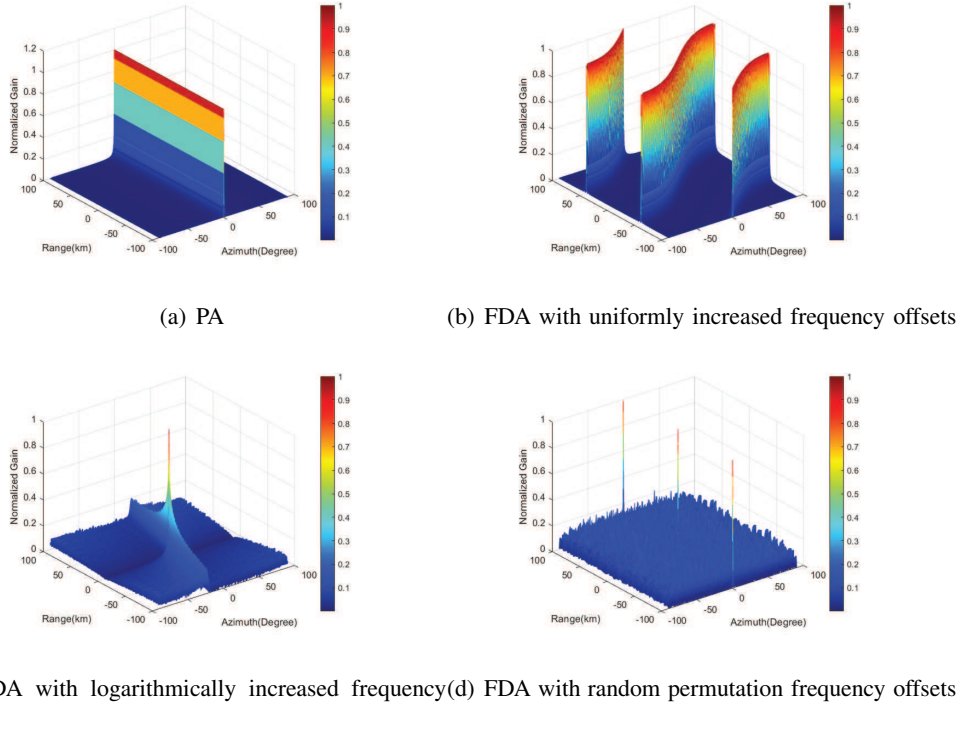


Fig. 2. Comparison of beam pattern between PA and different FDAs, where $M = 256$, $\delta f = 3$ kHz. To ensure the same maximum frequency offset, the logarithmically increased frequency offsets are set to $\delta f_m = (M - 1) \ln(m + 1) \delta f / \ln M$.

where $\mathbf{G}_1 = [0, 1/2, \dots, (M - 1)/2]^T$, $\mathbf{G}_2 = [0, -\delta f/c, \dots, -(M - 1) \delta f/c]^T$ and $l_1, \dots, l_{M-1} \in \mathbb{Z}$. Since \mathbf{G}_1 and \mathbf{G}_2 are linearly dependent, (R_j, θ_j) has infinite solutions to a fixed (R_i, θ_i) , leading to the coupling between distance and angle dimensions [32]. Therefore, breaking the dependency between \mathbf{G}_1 and \mathbf{G}_2 is crucial for generating focused beams in FDA. A simple and effective method is to randomly shuffle the elements in \mathbf{G}_2 by shuffling δf_m , which can be regarded as a special implementation of random frequency offsets. Fig. 2 illustrates the beam patterns of various frequency offsets. Among them, random permutation frequency offsets can generate nearly dot-shaped beams, exhibiting better two-dimensional directivity compared to logarithmically increasing frequency offsets, indicating that distance and angle have been successfully decoupled. Moreover, this frequency offset configuration maintains the same fast Fourier transform (FFT) characteristics in the distance domain as in the angle domain. Consequently, the beam patterns of both uniformly increased frequency offsets and random permutation frequency offsets exhibit periodicity. Based on the FFT property, the distance domain beamwidth equals $c / [(M - 1) \delta f]$, and the corresponding period equals $c / \delta f$.

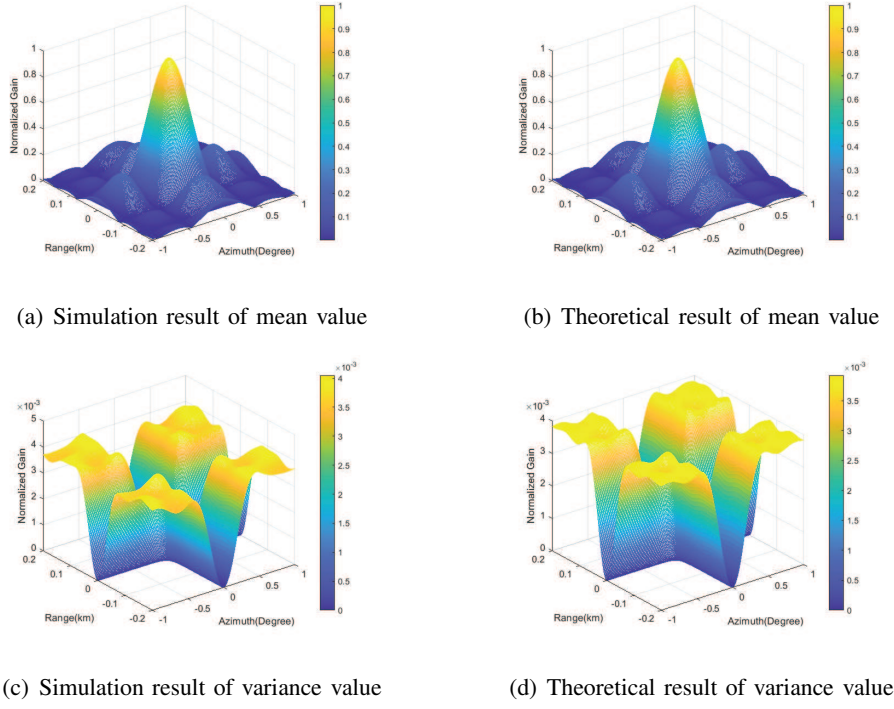


Fig. 3. The mean and variance results of beam correlation.

According to (21), we can easily obtain the clarified expression of correlation between two steering vectors at the same distance or angle. Due to the randomness of frequency offsets, precise computation of the correlation is unfeasible when $R_i \neq R_j$ and $\theta_i \neq \theta_j$. However, employing statistical properties allows for the analysis of the correlations between beams to some extent. Considering the correlation as a stochastic process with respect to distance and angle, it can be characterized by the following lemma.

Lemma 1. Let $\delta f_m = z_m \delta f$, where $z_m = \pi_m(\mathcal{M})$ denotes the m -th element in randomly shuffled sequence $\mathcal{M} = [0, 1, \dots, M-1]$. Then, the mean and variance of beams correlation $\eta_{i,j} = \mathbf{a}^H(R_i, \theta_i) \mathbf{a}(R_j, \theta_j)$ are given by

$$\mathbf{E}[\eta_{i,j}] = \text{Sa}_M(p_{i,j}) \text{Sa}_M(q_{i,j}) \exp \left\{ j\pi \frac{M-1}{M} (p_{i,j} - q_{i,j}) \right\}, \quad (23a)$$

$$\text{Var}[\eta_{i,j}] = \frac{1}{M} + \frac{M}{M-1} \left(\text{Sa}_M^2(p_{i,j}) - \frac{1}{M} \right) \left(\text{Sa}_M^2(q_{i,j}) - \frac{1}{M} \right) - \text{Sa}_M^2(p_{i,j}) \text{Sa}_M^2(q_{i,j}), \quad (23b)$$

where we denote $p_{i,j} = (\sin \theta_i - \sin \theta_j)/2$ and $q_{i,j} = \delta f (R_i - R_j) / c$.

Proof: Please refer to Appendix A. ■

To verify the accuracy of the moments of correlation, we illustrate a comparison between the theoretical

results and the simulation results in Fig. 3. All the simulations in the left column are counted from 1000 Monte Carlo trials, demonstrating a well match with the theoretical derivation. Then, the correlation can be approximated to

$$|\eta_{i,j}| \approx \sqrt{\frac{1}{M} + \frac{M}{M-1} \left(\text{Sa}_M^2(p_{i,j}) - \frac{1}{M} \right) \left(\text{Sa}_M^2(q_{i,j}) - \frac{1}{M} \right)}. \quad (24)$$

Based on the above analysis, we can prove the asymptotic orthogonality in the distance-angle domain in the following corollary.

Corollary 1. As the number of antennas increases, the steering vectors corresponding to any angle or distance in the FDA with random permutation frequency offsets approach asymptotically become orthogonal within one distance period.

$$\lim_{M \rightarrow +\infty} |\mathbf{a}^H(R_i, \theta_i) \mathbf{a}(R_j, \theta_j)| = 0, \quad \text{for } R_i \neq R_j \text{ or } \theta_i \neq \theta_j. \quad (25)$$

Proof: According to (24), as the number of antennas tends to infinity, the mean and variance of beta approach 0 when $R_i \neq R_j$ or $\theta_i \neq \theta_j$. Therefore, the correlation $\lim_{M \rightarrow +\infty} |\eta_{i,j}| = 0$, indicating asymptotic orthogonality of the steering vectors in the distance-angle domain. This completes the proof.

■

This corollary indicates that the FDA system with random permutation frequency offsets attains 2D orthogonality in the distance-angle domain, whereas the PA system achieves orthogonality solely in the angle domain. This property reveals that the FDA system can produce more channel DoFs in the spatial domain with the same number of transmitting antennas. Therefore, it provides the potential for the design of novel multiple access schemes, opening up possibilities for improving the spectral efficiency of existing MIMO systems.

B. Slight Frequency Offsets

While the FDA can satisfy the 2D asymptotic orthogonality of steering vectors, the trade-off is the introduction of ICIs as described in (10). We can observe that not only the phase of the received symbol is shifted, but also the interferences occur among distinct subcarriers across various antennas. A straightforward approach is to mitigate interference by employing slight frequency offsets to ensure the following condition

$$\int_0^{T_{\text{us}}} |g(t)|^2 \exp \{ -j2\pi(\ell' - \ell + \rho_m)\Delta ft \} dt \approx \begin{cases} 1, & \ell' \neq \ell, \\ 0, & \ell' = \ell, \end{cases} \quad (26)$$

so that the received symbol on the ℓ' -th subcarrier can be reduced to $y_{k,\ell',n} = \sum_{m=0}^{M-1} \mathbf{h}_{k,m,\ell'} \mathbf{x}_{\ell',m}$. The equivalent matrix form of (26) can be written as $\mathbf{F}_{N_{\text{us}}} \Xi \mathbf{F}_{N_{\text{us}}}^H \approx \mathbf{I}_{N_{\text{us}}}$, thus the system is capable of approximate orthogonal transmission as (18). Considering the assumption that UEs are aware of the precise location of the BS, UE can compensate for the phase shift $\exp(-j2\pi\ell\Delta f R_{k,0}/c)$ on each subcarrier in the received signal. As a result, it yields the ideal channel matrix $\bar{\mathbf{H}}^{\text{ideal}} = \mathbf{b}(\phi) \mathbf{a}^T(R, \theta) \otimes \mathbf{I}_{N_{\text{us}}}$ in the LoS path, and the vectorization form of the input-output relationship in FDA-MIMO-OFDM system becomes

$$\mathbf{y}_{k,\ell} = \sum_{p=0}^P \tilde{h}_{k,p} \mathbf{b}(\phi_{k,p}) \mathbf{a}^T(R_{k,p}, \theta_{k,p}) \mathbf{x}_{\ell}. \quad (27)$$

which is consistent with the traditional MIMO-OFDM model under multipath channels.

Nevertheless, the slighter frequency offsets will broaden the beamwidth in the distance domain, thereby reducing the resolution capability of the BS for different UE locations. Adopting symmetric frequency offsets can enhance the distance resolution while maintaining the same degree of ICIs. Let $\rho_{\text{max}} = \max \rho_m$ represent the ratio of the maximum frequency offset to the subcarrier spacing. Then, the basic frequency increment cell is $\delta f = 2\rho_{\text{max}}\Delta f/(M-1)$, and the frequency offsets are generated by randomly shuffling the sequence $[-(M-1)/2, -(M-1)/2+1, \dots, (M-1)/2] \delta f$. We compare the received symbols on each subcarrier with and without the addition of various frequency offsets in Fig. 4. When $\rho_{\text{max}} = 1/50$, the two signals are nearly indistinguishable, indicating that approximate orthogonal transmission can be achieved. As $\rho_{\text{max}} = 1/50$ increases to $1/20$, there is a slight deviation in the received symbols on the part of subcarriers. Significant deviation occurs when $\rho_{\text{max}} = 1/10$. At this point, it is necessary to eliminate ICIs to ensure correct system transmission. Taking the subcarrier spacings of 15 kHz and 240 kHz as examples, the beamwidth in the distance domain will reach 200 km and 12.5 km. Such wide beams may only have the possibility of application in satellite communications and it is far beyond the maximum propagation distance designed in Section II-A. Therefore, slight frequency offsets can not meet the design requirements of OFDM waveform, and can only consider the compatibility with other modulation systems, which is beyond the scope of this paper.

C. Pre-equalization

Another method to eliminate ICIs is to use equalization or pre-equalization. First, consider the case of employing pre-equalization. In the downlink, the BS first pre-equalizes the $MN_{\text{us}} \times 1$ -dimensional symbols before performing OFDM modulation. Likewise, assuming that UE can compensate the phase

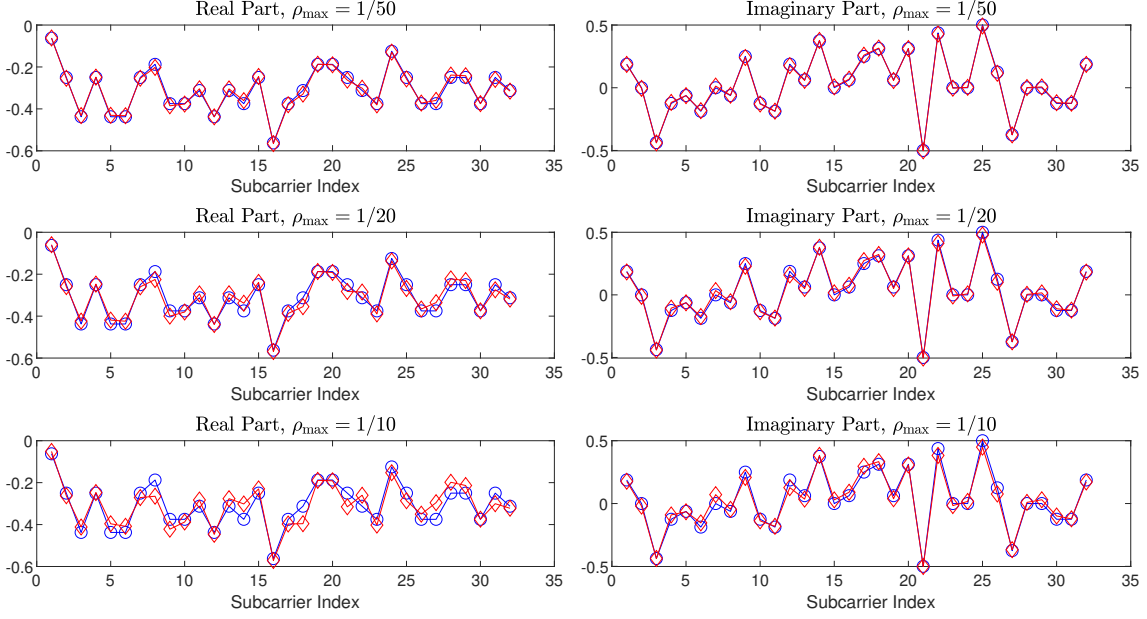


Fig. 4. The mean and variance results of beam correlation.

offset $\exp(-j2\pi\ell\Delta f R_{k,0}/c)$ based on BS position, the orthogonal transmission signal will be received on each subcarrier after matched filtering. With the total power constraint, the pre-equalization matrix $\mathbf{G}_P \in \mathbb{C}^{MN_{\text{us}} \times MN_{\text{us}}}$ is desired to satisfy

$$\begin{aligned} \min \quad & \|\bar{\mathbf{H}}_k \mathbf{G}_P - \bar{\mathbf{H}}_k^{\text{ideal}}\|_F^2, \\ \text{s.t.} \quad & \text{Tr}(\mathbf{G}_P^H \mathbf{G}_P) \leq MN_{\text{us}}, \end{aligned} \quad (28)$$

where $\bar{\mathbf{H}}_k = [\mathbf{b}(\phi_k) \mathbf{a}^T(R_k, \theta_k) \otimes \mathbf{F}_{N_{\text{us}}}] \mathbf{\Xi} (\mathbf{I}_M \otimes \mathbf{F}_{N_{\text{us}}}^H)$ is the compensated channel matrix under the LoS path, and $\|\cdot\|_F$ represents the Frobenius norm. The above optimization can be regarded as the MMSE problem without noise. For brevity, the optimal solution can be directly given by $\mathbf{G}_P^{\text{opt}} = \beta_P \tilde{\mathbf{G}}$, where $\tilde{\mathbf{G}} = (\bar{\mathbf{H}}_k^H \bar{\mathbf{H}}_k)^{-1} \bar{\mathbf{H}}_k^H \bar{\mathbf{H}}_k^{\text{ideal}}$ is the ZF solution and $\beta_P = \sqrt{MN_{\text{us}} / \text{Tr}(\tilde{\mathbf{G}}^H \tilde{\mathbf{G}})}$ is the gain control factor. The explicit expression for $\mathbf{G}_P^{\text{opt}}$ is given by the following corollary.

Corollary 2. Under the constraint of total power $\text{Tr}(\mathbf{G}_P^H \mathbf{G}_P) \leq N_{\text{us}}$, the optimal precoding matrix is given by $\mathbf{G}_P^{\text{opt}} = \text{diag}(\mathbf{F}_{N_{\text{us}}} \mathbf{\Xi}_0^{-1} \mathbf{F}_{N_{\text{us}}}^H, \mathbf{F}_{N_{\text{us}}} \mathbf{\Xi}_1^{-1} \mathbf{F}_{N_{\text{us}}}^H, \dots, \mathbf{F}_{N_{\text{us}}} \mathbf{\Xi}_{M-1}^{-1} \mathbf{F}_{N_{\text{us}}}^H)$.

Proof: Let's first calculate $(\bar{\mathbf{H}}_k^H \bar{\mathbf{H}}_k)^{-1}$ and $\bar{\mathbf{H}}_k^H \bar{\mathbf{H}}_k^{\text{ideal}}$ separately. The parameters R_k , θ_k and ϕ_k have been omitted here for simplicity. By utilizing the Kronecker product property, we have

$$\begin{aligned} (\bar{\mathbf{H}}_k^H \bar{\mathbf{H}}_k)^{-1} &= \left[(\mathbf{I}_M \otimes \mathbf{F}_{N_{\text{us}}}) \Xi^H [(\mathbf{b}\mathbf{a}^T)^H \otimes \mathbf{F}_{N_{\text{us}}}^H] [\mathbf{b}\mathbf{a}^T \otimes \mathbf{F}_{N_{\text{us}}}] \Xi (\mathbf{I}_M \otimes \mathbf{F}_{N_{\text{us}}}^H) \right]^{-1} \\ &= (\mathbf{I}_M \otimes \mathbf{F}_{N_{\text{us}}}) \Xi^{-1} [(\mathbf{b}\mathbf{a}^T)^{-1} (\mathbf{b}\mathbf{a}^T)^{-H} \otimes \mathbf{I}_{N_{\text{us}}}] \Xi^{-H} (\mathbf{I}_M \otimes \mathbf{F}_{N_{\text{us}}}^H), \end{aligned} \quad (29)$$

and

$$\begin{aligned} \bar{\mathbf{H}}_k^H \bar{\mathbf{H}}_k^{\text{ideal}} &= (\mathbf{I}_M \otimes \mathbf{F}_{N_{\text{us}}}) \Xi^H [(\mathbf{b}\mathbf{a}^T)^H \otimes \mathbf{F}_{N_{\text{us}}}^H] [\mathbf{b}\mathbf{a}^T \otimes \mathbf{I}_{N_{\text{us}}}] \\ &= (\mathbf{I}_M \otimes \mathbf{F}_{N_{\text{us}}}) \Xi^H [(\mathbf{b}\mathbf{a}^T)^H \mathbf{b}\mathbf{a}^T \otimes \mathbf{F}_{N_{\text{us}}}^H]. \end{aligned} \quad (30)$$

Combining with (29) and (30), $\tilde{\mathbf{G}}$ can be further simplified to a block diagonal matrix as follows

$$\begin{aligned} \tilde{\mathbf{G}} &= (\mathbf{I}_M \otimes \mathbf{F}_{N_{\text{us}}}) \Xi^{-1} [(\mathbf{b}\mathbf{a}^T)^{-1} (\mathbf{b}\mathbf{a}^T)^{-H} \otimes \mathbf{I}_{N_{\text{us}}}] [(\mathbf{b}\mathbf{a}^T)^H \mathbf{b}\mathbf{a}^T \otimes \mathbf{F}_{N_{\text{us}}}^H] \\ &= (\mathbf{I}_M \otimes \mathbf{F}_{N_{\text{us}}}) \Xi^{-1} (\mathbf{I}_M \otimes \mathbf{F}_{N_{\text{us}}}^H) \\ &= \text{diag} (\mathbf{F}_{N_{\text{us}}} \Xi_0^{-1} \mathbf{F}_{N_{\text{us}}}^H, \mathbf{F}_{N_{\text{us}}} \Xi_1^{-1} \mathbf{F}_{N_{\text{us}}}^H, \dots, \mathbf{F}_{N_{\text{us}}} \Xi_{M-1}^{-1} \mathbf{F}_{N_{\text{us}}}^H). \end{aligned} \quad (31)$$

Since $(\mathbf{F}_{N_{\text{us}}} \Xi_m^{-1} \mathbf{F}_{N_{\text{us}}}^H)^H \mathbf{F}_{N_{\text{us}}} \Xi_m^{-1} \mathbf{F}_{N_{\text{us}}}^H = \mathbf{I}_{N_{\text{us}}}$, we immediately obtain $\beta_P = \sqrt{MN_{\text{us}}/\text{Tr}(\mathbf{I}_{MN_{\text{us}}})} = 1$, which completes the proof. \blacksquare

Obviously, the optimal $\mathbf{G}_P^{\text{opt}}$ satisfies $\bar{\mathbf{H}}_k \mathbf{G}_P^{\text{opt}} = \bar{\mathbf{H}}_k^{\text{ideal}}$. Substituting $\mathbf{G}_P^{\text{opt}}$ into the FDA-MIMO-OFDM model yields the input-output relationship as shown in (27).

Let's now consider implementing an equalization strategy. While it is unnecessary to impose power constraints at the receiving end, the equalizer will modify the characteristics of the noise distribution. Utilizing the MMSE criterion, we can directly obtain the optimal equalization matrix as $\mathbf{G}_E^{\text{opt}} = \bar{\mathbf{H}}_k^{\text{ideal}} \bar{\mathbf{H}}_k^H (\bar{\mathbf{H}}_k \bar{\mathbf{H}}_k^H + \sigma_n^2 \mathbf{I}_{NN_{\text{us}}})^{-1}$. It is evident that computing $\mathbf{G}_E^{\text{opt}}$ requires a full CSI at the receiver, which markedly increases the complexity relative to pre-equalization scheme.

IV. PERFORMANCE ANALYSIS OF LDMA

Although it has been established that steering vectors with randomly permuted frequency offsets achieve asymptotic orthogonality across the distance-angle plane, this does not lead to an increase in DoFs relative to traditional SDMA systems. Given that an array consisting of M elements can only support up to M mutually orthogonal vectors, inter-user interferences persist among UEs positioned at varying angles and distances when M remains finite. Furthermore, the introduction of frequency offsets contributes to increased overhead in channel resource utilization. Therefore, the potential of LDMA to enhance spectral efficiency in MIMO systems needs more detailed examination and discussion.

Since the received steering vectors of LDMA and SDMA are identical, without loss of generality, we consider single-antenna UE for convenience of performance comparison. After adopting the ideal channel

matrix, the dimension corresponding to the subcarrier in the MU-MIMO model described in (20) can be discarded. In this way, the channel matrix for the k -th UE will degenerate to a K -dimensional vector, which is given by $\mathbf{h}_k^T = \sum_{p=0}^P \tilde{h}_{k,p} \mathbf{a}^T(R_{k,p}, \theta_{k,p})$, and the corresponding MU-MIMO channel model will become to $\bar{\mathbf{H}} = [\mathbf{h}_0, \mathbf{h}_1, \dots, \mathbf{h}_{K-1}]^T \in \mathbb{C}^{K \times M}$. It follows that the transmit symbols degenerate to $\mathbf{s} = [s_0, s_1, \dots, s_{K-1}] \in \mathbb{C}^{K \times 1}$, and the received symbols similarly degenerate to $\mathbf{y} = [y_0, y_1, \dots, y_{K-1}] \in \mathbb{C}^{K \times 1}$. Then, ergodic spectrum efficiency in the downlink could be expressed as

$$R^{\text{LDMA}} = \frac{N_{\text{us}}}{N_{\text{us}} + \rho_{\text{max}}} \sum_k \mathbf{E}_{\bar{\mathbf{H}}} [R_k^{\text{LDMA}}] = \frac{N_{\text{us}}}{N_{\text{us}} + \rho_{\text{max}}} \mathbf{E}_{\bar{\mathbf{H}}} \left[\sum_k \log_2 \left(1 + \frac{|a_k \mathbf{h}_k^T \mathbf{w}_k|^2}{\sum_{i \neq k} |a_i \mathbf{h}_k^T \mathbf{w}_i|^2 + \sigma_n^2} \right) \right]. \quad (32)$$

MMSE precoding is a commonly employed strategy in downlink multi-user MIMO transmissions, where the transmit precoding vector for each k -th UE is determined by

$$\mathbf{w}_k = \frac{1}{\beta_{\text{MMSE}}} \left(\bar{\mathbf{H}}^H \bar{\mathbf{H}} + \frac{K \sigma_n^2}{P} \right)^{-1} \mathbf{h}_k, \quad (33)$$

where β_{MMSE} is the power normalization factor that is set to satisfy $\|\mathbf{w}_k\| = 1$. With equal power allocation, the resulting SINR value can be given by [33]

$$\text{SINR}_k = \frac{\gamma}{\left[\left(\bar{\mathbf{H}} \bar{\mathbf{H}}^H + \frac{1}{\gamma} \mathbf{I}_K \right)^{-1} \right]_{k,k}} - 1, \quad (34)$$

where $\gamma = \sum_k a_k^2 / (K \sigma_n^2)$ is the SNR of each UE.

Suppose that UEs are uniformly distributed within a sector-shaped region defined by distances from 0 to R_{max} and angles from $-\theta_{\text{max}}$ to θ_{max} , where R_{max} is less than one period of the distance domain and also less than the maximum coverage range permitted by the designed system. In (34), calculating the SINR for each UE involves inverting matrix $\bar{\mathbf{H}} \bar{\mathbf{H}}^H + 1/\gamma \mathbf{I}_K$. We commence by investigating the spectral efficiency by considering the two UEs and each UE operates on a single-path channel for simplicity. Then, the ergodic spectral efficiency can be formulated by the following lemma.

Lemma 2. With MMSE precoding and equal power allocation, the ergodic spectrum efficiency of two UEs in a single-path channel can be approximately upper-bounded by

$$R^{\text{LDMA, two UEs}} \leq \frac{2N_{\text{us}}}{N_{\text{us}} + \rho_{\text{max}}} \log_2 \frac{(\gamma + 1)^2 - \gamma^2 / (M - 1)}{1 + \gamma}. \quad (35)$$

Proof: Considering two UEs located at (R_1, θ_1) and (R_2, θ_2) , we have

$$\bar{\mathbf{H}} \bar{\mathbf{H}}^H + \frac{1}{\gamma} \mathbf{I}_K = \begin{bmatrix} 1 + \frac{1}{\gamma} & \eta_{1,2} \\ \eta_{2,1} & 1 + \frac{1}{\gamma} \end{bmatrix}. \quad (36)$$

Then, the diagonal entries of the inversed matrix are both equal to $(1 + 1/\gamma) / \left((1 + 1/\gamma)^2 - |\eta_{1,2}|^2 \right) - 1$, and the spectral efficiency of the two UEs is given by

$$\begin{aligned} R^{\text{LDMA, two UEs}} &= \frac{2N_{\text{us}}}{N_{\text{us}} + \rho_{\text{max}}} \mathbf{E}_{\bar{\mathbf{H}}} \left[\log_2 \frac{\gamma \left((1 + 1/\gamma)^2 - |\eta_{1,2}|^2 \right)}{1 + 1/\gamma} \right] \\ &\stackrel{a}{\leq} \frac{2N_{\text{us}}}{N_{\text{us}} + \rho_{\text{max}}} \log_2 \frac{\gamma \left((1 + 1/\gamma)^2 - \mathbf{E}_{\bar{\mathbf{H}}} \left[|\eta_{1,2}|^2 \right] \right)}{1 + 1/\gamma}, \end{aligned} \quad (37)$$

where (a) follows from Jensen's inequality, and $\mathbf{E}_{\bar{\mathbf{H}}} \left[|\eta_{1,2}|^2 \right]$ can be calculated as

$$\mathbf{E}_{\bar{\mathbf{H}}} \left[|\eta_{1,2}|^2 \right] = \int_0^{R_{\text{max}}} \int_{\theta_{\text{max}}}^{\theta_{\text{max}}} p(R_1 - R_2, \sin \theta_1 - \sin \theta_2) |\eta_{1,2}|^2 d(R_1 - R_2) d(\sin \theta_1 - \sin \theta_2) \stackrel{a}{\approx} \frac{1}{M - 1}, \quad (38)$$

where the approximation (a) is obtained by $|\eta_{i,j}| \approx 1/(M - 1)$ for most paired (R_1, θ_1) and (R_2, θ_2) , given the extremely low probability of two UEs being located in the same direction or at the same distance. Substituting (38) into (37), we can obtain (35), which completes the proof. ■

Meanwhile, we are interested in whether LDMA enhances system capacity compared to SDMA. Observing (37), the spectral efficiency is equivalent to that of SDMA when $\delta f = 0$. Since the number of subcarriers N_{us} does not affect the calculation of SINR, the frequency offsets overhead of LDMA with infinite bandwidth can be negligible. Along with the above analysis, the gap between the two systems can be compared directly by the beam correlation.

Corollary 3. In a single-path downlink channel with infinite bandwidth, the LDMA with 2 UEs outperforms SDMA in spectral efficiency when $\text{Sa}_M^2((\sin \theta_1 - \sin \theta_2)/2) > 1/M$ is satisfied.

Proof: The beam correlation of SDMA can be directly determined by $|\eta_{1,2}^{\text{SDMA}}|^2 = \text{Sa}_M^2(p_{1,2})$, so we can make the following comparison

$$\begin{aligned} |\eta_{1,2}^{\text{LDMA}}|^2 - |\eta_{1,2}^{\text{SDMA}}|^2 &= \frac{1}{M} + \frac{M}{M - 1} \left(\text{Sa}_M^2(p_{1,2}) - \frac{1}{M} \right) \left(\text{Sa}_M^2(q_{1,2}) - \frac{1}{M} \right) - \text{Sa}_M^2(p_{1,2}) \\ &= \left(\frac{M \text{Sa}_M^2(p_{1,2}) - 1}{M - 1} \right) (\text{Sa}_M^2(q_{1,2}) - 1). \end{aligned} \quad (39)$$

The performance of LDMA exceeds that of SDMA when $|\eta_{1,2}^{\text{LDMA}}|^2 < |\eta_{1,2}^{\text{SDMA}}|^2$. Since $\text{Sa}_M^2(q_{1,2}) - 1 \leq 0$, it means $\text{Sa}_M^2((\sin \theta_1 - \sin \theta_2)/2) > 1/M$ needs to be satisfied, which completes the proof. ■

Corollary 3 illustrates that in a downlink scenario with only two UEs, the performance of the LDMA system surpasses that of SDMA only when the UEs are located within a certain threshold of θ_{max} .

Subsequently, we further analyze the spectrum efficiency of multiple UEs. At this point, $|\eta_{i,j}|^2$ cannot be briefly approximated as $1/M$. To our best knowledge, it is still intractable to derive an analytical

solution for the diagonal elements of such inversed Hermitian matrices. The statistical properties of $\left[(\bar{\mathbf{H}}\bar{\mathbf{H}}^H + 1/\gamma\mathbf{I}_K)^{-1} \right]_{k,k}$ in the case of $\bar{\mathbf{H}}$ being i.i.d. Gaussian matrix have been analyzed in [34]. The maximum spectrum efficiency of multiple UEs can be approximatively obtained through the following lemma.

Lemma 3. With the high SNR assumption, the spectral efficiency of LDMA can be approximately upper-bounded by

$$R^{\text{LDMA}} \leq \frac{KN_{\text{us}}}{N_{\text{us}} + \rho_{\text{max}}} \log_2 \frac{\gamma(M - K + 1)}{M}. \quad (40)$$

Proof: Using Jensen's inequality, we can obtain

$$\begin{aligned} R^{\text{LDMA}} &\stackrel{\text{High SNR}}{\approx} \frac{N_{\text{us}}}{N_{\text{us}} + \rho_{\text{max}}} \sum_k \mathbf{E}_{\bar{\mathbf{H}}} \left[\log_2 \frac{\gamma}{[(\bar{\mathbf{H}}\bar{\mathbf{H}}^H)^{-1}]_{k,k}} \right] \\ &\leq \frac{N_{\text{us}}}{N_{\text{us}} + \rho_{\text{max}}} \sum_k \log_2 \left(\gamma \mathbf{E}_{\bar{\mathbf{H}}} \left[\frac{1}{[(\bar{\mathbf{H}}\bar{\mathbf{H}}^H)^{-1}]_{k,k}} \right] \right). \end{aligned} \quad (41)$$

As indicated in [35], if the channel correlation between different UEs is 0 and the independence between array elements holds in an MU-MIMO channel, it follows that $\mathbf{E}_{\bar{\mathbf{H}}} [1/[(\bar{\mathbf{H}}\bar{\mathbf{H}}^H)^{-1}]_{k,k}] = (M - K + 1)/K$. Obviously, the UEs are independently distributed, thus satisfying the condition of correlation. As for $\mathbf{E}_{\bar{\mathbf{H}}} [\mathbf{h}_i^H \mathbf{h}_i]$, the diagonal elements are absolutely $1/M$, and the elements in the n -th row and m -th column can be expressed by

$$\mathbf{E}_{\bar{\mathbf{H}}} [\mathbf{h}_i^H \mathbf{h}_i]_{n,m} = \mathbf{E}_{\bar{\mathbf{H}}} \left[\sum_p \sum_l h_l^* h_p \exp \{j\pi(m \sin \theta_p - n \sin \theta_l)\} \exp \left\{ j2\pi\delta f \frac{R_l z_n - R_p z_m}{c} \right\} \right]. \quad (42)$$

Since all variables in (42) are independent and R_p follows uniform distribution, we can immediately obtain $\mathbf{E}_{\bar{\mathbf{H}}} [\mathbf{h}_i^H \mathbf{h}_i]_{n,m} = 0$, which completes the proof. ■

Additionally, it is apparent that (42) still holds under a single-path channel. This finding highlights that LDMA's system performance is inherently independent of multipath channel effects, which facilitates full MIMO channel degrees of freedom for multiple access. Such a characteristic is particularly advantageous in the millimeter-wave and higher frequency domains, where multipath effects can severely limit the capabilities of SDMA systems.

V. SIMULATION RESULTS

In this section, we evaluate the performance of the proposed far-field LDMA scheme through numerical simulations. To satisfy the approximation in (6), the carrier frequency is set to 30 GHz. The array is configured with a half-wavelength spacing, resulting in a distance of $d = 0.5\text{cm}$. The subcarrier

spacing is set to be 15 kHz with $N_{\text{us}} = 512$, and the CP length is 1/4 OFDM symbol period, which is about $16.67\mu\text{s}$. As outlined in Section II-A, the coverage area of the designed system should ensure that the maximum channel propagation delay remains within the confines of the CP length. Assuming the maximum multipath delay spread is $6.67\mu\text{s}$, it yields a maximum LoS coverage distance of 3 km for the BS. Therefore, the UEs are set to be uniformly distributed within the sector area defined by $\theta \in [-\theta_{\text{max}}, \theta_{\text{max}}]$ and $R \in [0, 3\text{km}]$. The BS is equipped with a ULA of 128 elements, while the UEs are equipped with a single antenna in simulations. Assuming that the ICIs yielded by frequency offsets and the phase shifts of subcarriers caused by STO can be perfectly compensated using the aforementioned methods, we can obtain the ideal channel model for FDA-MIMO baseband signals. To validate our derivations and demonstrate the superior performance of the proposed LDMA, two scenarios are considered including two UEs under the single-path channel and multiple UEs under the multipath channel. All simulations come from 10,000 Monte Carlo samples.

A. Two UEs under the Single-path Channel

First, the curves of spectral efficiency versus SNRs are plotted in Fig. 5. We establish two simulations where the coverage angles of the BS are $[-5^\circ, 5^\circ]$ and $[-20^\circ, 20^\circ]$. In each simulation, we consider three frequency offset ratios $\rho_{\text{max}} = 1, 10, 50$, corresponding to distance-domain beam resolutions of 20 km, 2 km, and 400 m, respectively. The red represents the simulation results, and the blue lines are evaluated by (35). We can notice that as θ_{max} or ρ_{max} increases, the driver upper bound gradually becomes tighter. With a larger θ_{max} , the probability of different UEs being located in the same direction or at the same distance decreases, thereby rendering the approximation $|\eta_{i,j}| \approx 1/(M-1)$ more reasonable. Likewise, the beam resolution in the distance domain will improve as ρ_{max} increases, so the BS acquires a higher precision to distinguish between UEs that are close to each other. Furthermore, the simulated spectral efficiency for $\rho_{\text{max}} = 10$ at $\theta_{\text{max}} = 5^\circ$ is slightly higher than that for $\rho_{\text{max}} = 1$, whereas the opposite is true at $\theta_{\text{max}} = 20^\circ$. This observation implies that there exists an ideal value of ρ_{max} that maximizes system performance within the constraints of a specified θ_{max} , pointing to the demand for parameter tuning for optimal transmission. Moreover, the spectral efficiency for $\rho_{\text{max}} = 50$ is the lowest, indicating that higher distance resolution does not necessarily provide better system performance. The fundamental reason is that the SINR gains afforded by a larger ρ_{max} fail to offset the spectral losses.

To further explore the performance of LDMA, the spectrum efficiency with increasing θ_{max} under various values for ρ_{max} is shown in Fig. 6, and makes a comparison with SDMA. SNR is set to be 20 dB. When $\theta_{\text{max}} \leq 3^\circ$, particularly at $\theta_{\text{max}} = 0^\circ$ where UEs are aligned in a straight line, the

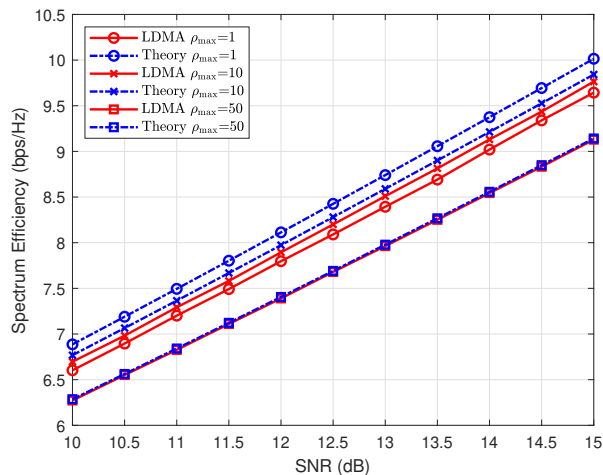
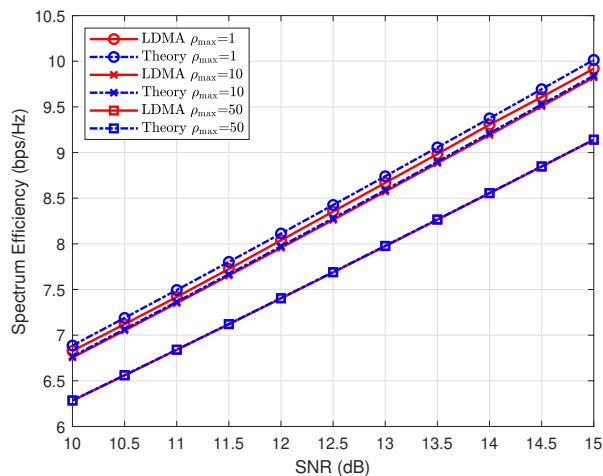
(a) $\theta_{\max} = 5^\circ$ (b) $\theta_{\max} = 20^\circ$

Fig. 5. Spectral efficiency achieved in a single-path channel in LDMA system consisting of two UEs.

performance of the LDMA system with $\rho_{\max} = 10$ and $\rho_{\max} = 50$ substantially surpasses that of SDMA. This demonstrates LDMA's advanced capability to effectively reduce inter-user interferences under such location configurations. However, once $\theta_{\max} \geq 15^\circ$, the spectral efficiency of SDMA will exceed that of the above two systems, which is consistent with **Corollary 3**. One aspect is that while interference in SDMA diminishes as the angle between UEs increases, the interference in our proposed LDMA remains relatively stable even with an increase in the Euclidean distance between UEs, unless they coincide at the same angle or distance. On the other hand, LDMA has extra spectral overhead, inherently placing

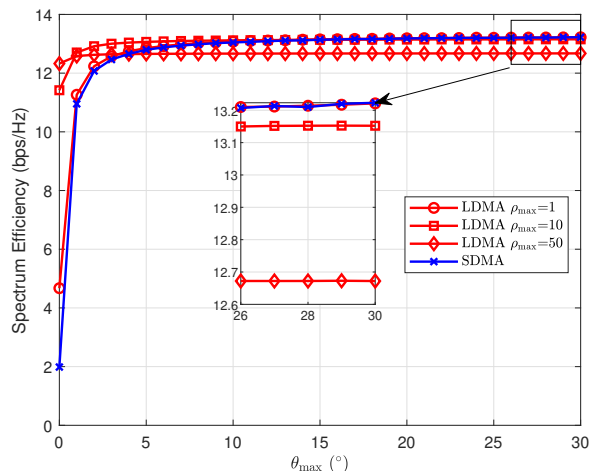


Fig. 6. Comparison of the proposed LDMA with various ρ_{\max} and SDMA for different θ_{\max} in a system with two UEs.

it at a disadvantage in scenarios with fewer users. Given that UEs are situated within the confines of a single beamwidth of distance domain, it becomes evident that the performance of the LDMA system with $\rho_{\max} = 1$ closely matches that of SDMA, exhibiting a more significant performance improvement only at $\theta_{\max} = 0^\circ$. If UEs are permitted to be distributed across a wider distance, employing $\rho_{\max} = 1$ can significantly increase the BS's probability of successfully distinguishing between two UEs' locations, leading to enhanced spectral efficiency. From this, it follows that under the conditions of a specified number of subcarriers and UE distribution range, there theoretically exists an optimal ρ_{\max} .

B. Multiple UEs under the Multipath channel

To validate the performance improvement of the proposed LDMA over SDMA in multiple UEs scenarios, we first depict the spectral efficiency of systems using MMSE and ZF precoding under a single-path channel Fig. 6. The SNR is configured at 30 dB, and $\rho_{\max} = 30$. UEs are distributed within a sector spanning from -60° to 60° degrees. The theoretical bound derived from **Lemma 3** is plotted with a black dashed line. We observe that LDMA's spectral efficiency begins to surpass that of SDMA once the number of UEs exceeds 10. For SDMA with ZF precoding, spectral efficiency starts to decline when the number of UEs reaches 30 and tends toward zero upon reaching 80. Even with MMSE precoding, SDMA's spectral efficiency only increases slowly as the number of UEs grows. However, the spectral efficiency of LDMA systems utilizing ZF and MMSE precoding increases rapidly and aligns closely with theoretical values until the number of UEs reaches 100. There is a noticeable divergence from the theoretical bound

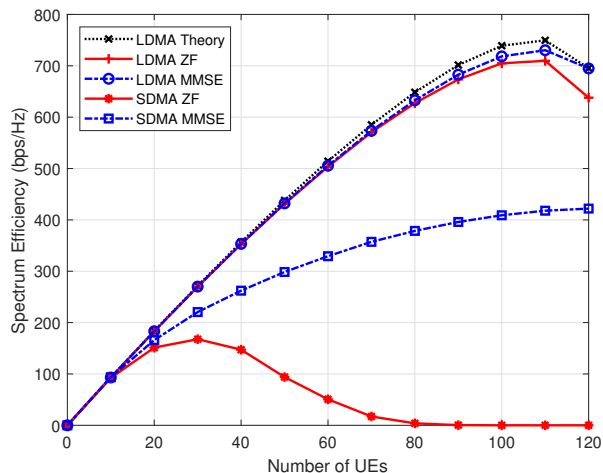


Fig. 7. Comparison of the proposed LDMA and SDMA for different numbers of UEs under single-path channel.

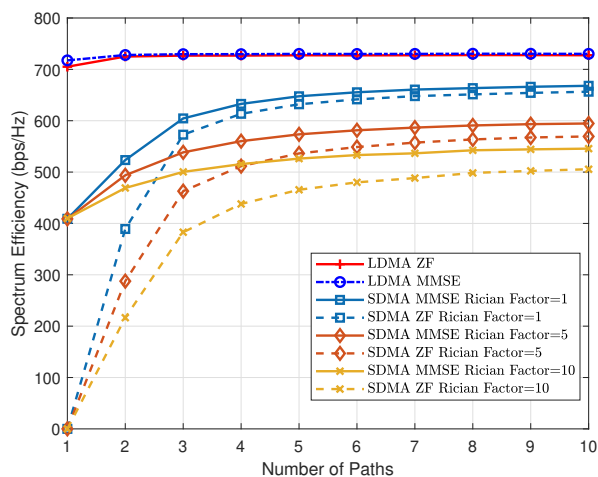


Fig. 8. Comparison of the proposed LDMA and SDMA for different numbers of path channels.

only when the UE count exceeds 80. Therefore, the proposed LDMA can provide about 75% performance gain compared with SDMA at SNR=30 dB. The substantial performance improvement can be attributed to LDMA's ability to effectively distinguish UEs at different distances. However, the fundamental reason lies in the newly designed steering vectors, which exhibit more uniform beam correlation across each pair of UEs compared to traditional PA steering vectors. In the SDMA system, the steering vectors exhibit high correlation when the angles between two UEs are close, resulting in some very small eigenvalues of $\bar{\mathbf{H}}\bar{\mathbf{H}}^H$. This is reflected in the inversed matrix where some diagonal elements become significantly large.

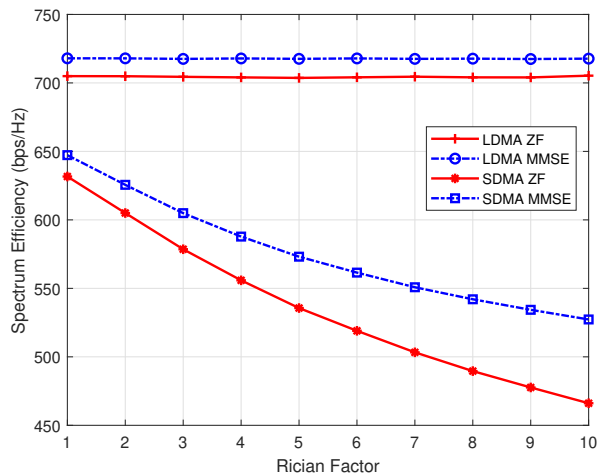
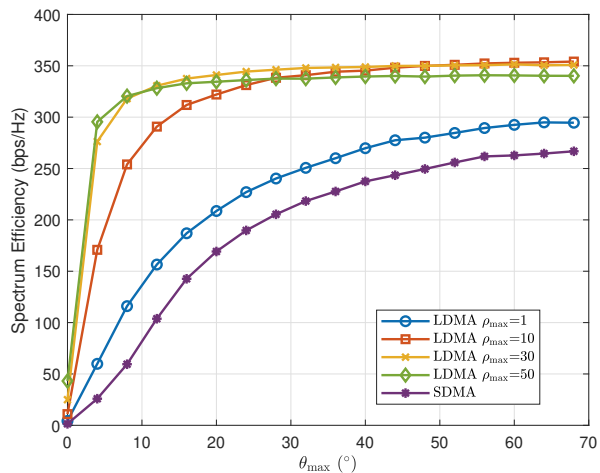


Fig. 9. Comparison of the proposed LDMA and SDMA for different Rician factors.

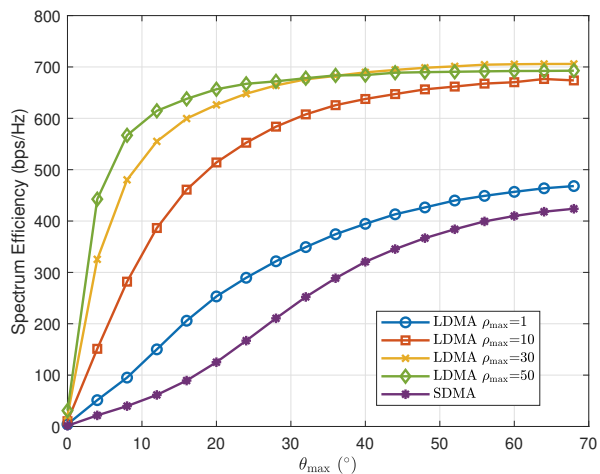
During the Frobenius norm normalization process, a considerable amount of transmit power is allocated to these larger diagonal elements, leading to substantial disparities in the SINR among UEs. Conversely, the diagonal elements of the inversed matrix are relatively uniform in LDMA, thereby achieving higher spectral efficiency.

In Fig. 8, we compare the performance of LDMA and SDMA among 100 UEs across different numbers of paths P . With the increase of P , the spectral efficiency of SDMA gradually increases, while that of LDMA remains constant. Additionally, it becomes apparent that the performance of SDMA progressively deteriorates as the Rician factor increases. This is better illustrated in Fig. 9, where it is evident that LDMA's performance is mostly unaffected by changes in the Rician factor. The underlying reasons for these phenomena are that the channel matrix elements of SDMA gradually conform to i.i.d. Gaussian due to the Central Limit Theorem in rich scattering environments. As a result, SDMA's performance continues to improve with the increasing P . Conversely, LDMA's channel matrix meets the independence conditions even in a single-path scenario, which is why the performance of LDMA tends towards the upper bound as shown in Fig. 7. This indicates that LDMA's system performance does not depend on multipath effects, thereby enabling ideal spectral efficiency in millimeter waves.

Finally, we further explored the variation of spectral efficiency by adjusting θ_{\max} and R_{\max} . Fig. 10 elucidates that there consistently emerges an optimal value for ρ_{\max} that is capable of optimizing spectral efficiency across a spectrum of angular settings and varying numbers of UEs. A similar phenomenon is also evident when altering R_{\max} , as demonstrated in Fig. 11. As previously mentioned, the performance



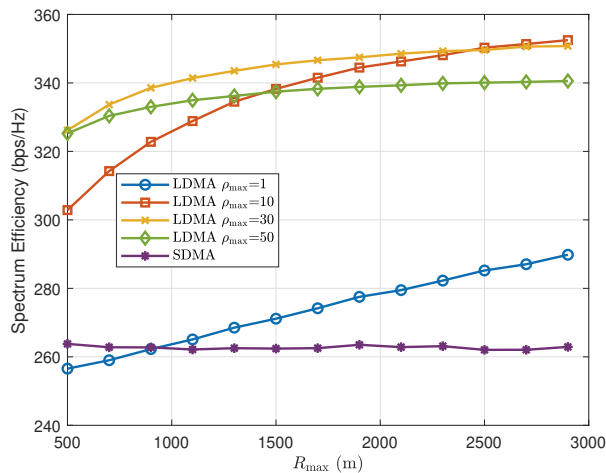
(a) 40 UEs



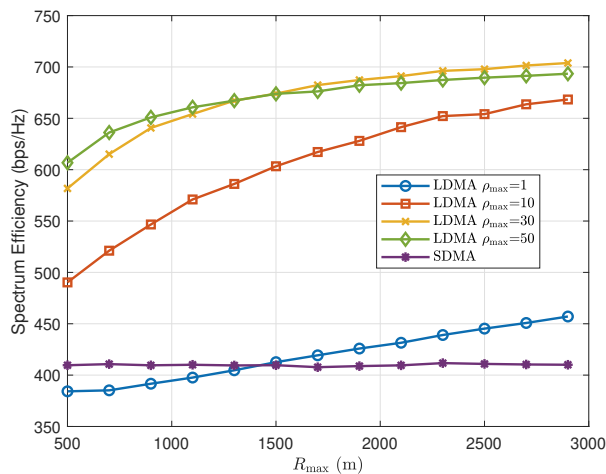
(b) 100 UEs

Fig. 10. Spectral efficiency versus θ_{\max} for proposed LDMA with various ρ_{\max} and SDMA.

enhancements of LDMA stem from its ability to distribute interference more evenly. Elevating ρ_{\max} serves to narrow the mainlobe width in the two-dimensional plane, reducing the probability of UEs sharing the same beam and thus boosting spectral efficiency. However, increasing ρ_{\max} also leads to a rise in frequency overhead. It follows that under specific conditions for θ_{\max} , R_{\max} and the number of UEs, there exists an optimal value of ρ_{\max} that can maximize spectral efficiency. Moreover, as shown in Fig. 10, it can be observed that the spectral efficiency initially increases sequentially with the rise of θ_{\max} , and then converges beyond a certain threshold. Therefore, LDMA exhibits several times the spectral efficiency of



(a) 40 UEs



(b) 100 UE

Fig. 11. Spectral efficiency versus R_{\max} for proposed LDMA with various ρ_{\max} and SDMA.

SDMA in ultra-dense networks with narrow sectors. A consequent idea is to adopt LDMA after dividing the cellular network into smaller sectors, which can significantly improve the system capacity of the BS.

VI. CONCLUSION

In this paper, we propose a far-field LDMA scheme based on the ability of the FDA to manipulate far-field beams in the distance domain. By using random permutation frequency offsets, the steering vectors also satisfy asymptotic orthogonality in the distance-angle domain. A pre-equalization method is proposed to eliminate ICIs caused by frequency offsets, which can achieve ideal orthogonal transmission in the

MU-MIMO system. Simulation results show that the proposed LDMA scheme has significant spectral efficiency advantages, especially in narrow sector multiple communication scenarios. The independence between antennas in LDMA makes it highly promising for future millimeter-wave and higher-frequency communication systems. For future research, since the design principles of OFDM limit the maximum coverage of LDMA, other waveforms compatible with FDA need to be considered for longer-distance communications. Furthermore, the optimal ρ_{\max} for different communication scenarios is another important direction for future research.

ACKNOWLEDGMENT

APPENDIX A

PROOF OF LEMMA 1

The beam correlation using random permutation frequency offsets can be calculated as

$$\eta_{i,j} = \frac{1}{M} \sum_{m=0}^{M-1} \exp \left\{ j2\pi \left[m \left(\frac{\sin \theta_i - \sin \theta_j}{2} \right) - z_m \left(\delta f \frac{R_i - R_j}{c} \right) \right] \right\}. \quad (43)$$

Since z_m is a random sampling variable, the mean of $\eta(q_{i,j}, p_{i,j})$ can be calculated as

$$\begin{aligned} \mathbf{E}[\eta(q_{i,j}, p_{i,j})] &= \int_{\mathbf{z} \in \mathcal{M}^M} p(\mathbf{z}) \eta(q_{i,j}, p_{i,j}) d\mathbf{z} \\ &= \int_{\mathbf{z} \in \mathcal{M}^M} p(z_m | \mathbf{z} \setminus z_m) p(\mathbf{z} \setminus z_m) \eta(q_{i,j}, p_{i,j}) d\mathbf{z} \\ &= \frac{1}{M} \sum_{m=0}^{M-1} \exp \{j2\pi m q_{i,j}\} \int_{\mathbf{z} \in \mathcal{M}^M} p(z_m | \mathbf{z} \setminus z_m) p(\mathbf{z} \setminus z_m) \exp \{-j2\pi z_m p_{i,j}\} dz_m d\mathbf{z} \setminus z_m \\ &\stackrel{(a)}{=} \frac{1}{M} \sum_{m=0}^{M-1} \exp \{j2\pi m q_{i,j}\} \frac{1}{M} \sum_{m=0}^{M-1} \exp \{j2\pi z_m p_{i,j}\} \\ &= \text{Sa}_M(q_{i,j}) \text{Sa}_M(p_{i,j}) \exp \left\{ j\pi \frac{M-1}{M} (p_{i,j} - q_{i,j}) \right\}. \end{aligned} \quad (44)$$

where $\mathbf{z} \setminus z_m$ represents all the elements of \mathbf{z} outside z_m . For a randomly shuffled sequence, it holds that $p(z_m | \mathbf{z} \setminus z_m) = 1$ and $p(\mathbf{z} \setminus z_m) = 1/M!$. Therefore, equation (a) can be obtained. The variance of $\eta(q_{i,j}, p_{i,j})$ can be obtained by

$$\begin{aligned} \text{Var}[\eta_{i,j}] &= \mathbf{E} \left[|\eta_{i,j}|^2 \right] - \frac{1}{M^2} |\mathbf{E}[\eta_{i,j}]|^2 \\ &= \frac{1}{M} + \sum_{m=0}^{M-1} \sum_{n=0, n \neq m}^{M-1} \exp \{j\pi (m-n) p_{i,j}\} \mathbf{E}[\exp \{j\pi (z_m - z_n) q_{i,j}\}] - |\mathbf{E}[\eta_{i,j}]|^2, \end{aligned} \quad (45)$$

where

$$\begin{aligned}
& \mathbf{E}[\exp\{j\pi(z_m - z_n)q_{i,j}\}] \\
&= \int_{\mathbf{z}_m \in \mathcal{M}^M, \mathbf{z}_n \in (\mathcal{M} \setminus z_m)^{M-1}} p(\mathbf{z}_m)p(\mathbf{z}_n) \exp\{j\pi(z_m - z_n)q_{i,j}\} d\mathbf{z}_m d\mathbf{z}_n \\
&= \int_{\mathbf{z}_n \in \mathcal{M}^M} \frac{1}{M!} d\mathbf{z}_m \setminus z_m \int_{\mathbf{z}_n \in (\mathcal{M} \setminus z_m)^{M-1}} \frac{1}{(M-1)!} d\mathbf{z}_n \setminus z_n \sum_{m=0}^{M-1} \sum_{n=0, n \neq m}^{M-1} \exp\{j\pi(z_m - z_n)q_{i,j}\} \\
&= \frac{1}{M} \frac{1}{(M-1)} \left(\sum_{m=0}^{M-1} \sum_{n=0}^{M-1} \exp\{j\pi(z_m - z_n)q_{i,j}\} - M \right) \\
&= \frac{M}{M-1} \left(\text{Sa}_M^2(q_{i,j}) - \frac{1}{M} \right).
\end{aligned} \tag{46}$$

Substituting (46) into (45), the $\mathbf{Var}[\eta_{i,j}]$ can be further rewritten as

$$\mathbf{Var}[\eta_{i,j}] = \frac{1}{M} + \frac{M}{M-1} \left(\text{Sa}_M^2(q_{i,j}) - \frac{1}{M} \right) \left(\text{Sa}_M^2(p_{i,j}) - \frac{1}{M} \right) - \text{Sa}_M^2(q_{i,j})\text{Sa}_M^2(p_{i,j}). \tag{47}$$

this completes the proof of **Lemma 1**.

REFERENCES

- [1] W. Saad, M. Bennis, and M. Chen, "A vision of 6g wireless systems: Applications, trends, technologies, and open research problems," *IEEE Network*, vol. 34, no. 3, pp. 134–142, 2020.
- [2] B. Clerckx, Y. Mao, Z. Yang, M. Chen, A. Alkhateeb, L. Liu, M. Qiu, J. Yuan, V. W. S. Wong, and J. Montojo, "Multiple access techniques for intelligent and multi-functional 6g: Tutorial, survey, and outlook," *arXiv preprint arXiv:2401.01433*, 2024.
- [3] Y. Liu, C. Ouyang, Z. Ding, and R. Schober, "The road to next-generation multiple access: A 50-year tutorial review," *arXiv preprint arXiv:2403.00189*, 2024.
- [4] E. G. Larsson, O. Edfors, F. Tufvesson, and T. L. Marzetta, "Massive mimo for next generation wireless systems," *IEEE Communications Magazine*, vol. 52, no. 2, pp. 186–195, 2014.
- [5] M. Agiwal, A. Roy, and N. Saxena, "Next generation 5g wireless networks: A comprehensive survey," *IEEE Communications Surveys & Tutorials*, vol. 18, no. 3, pp. 1617–1655, 2016.
- [6] A. Tarighat, M. Sadek, and A. Sayed, "A multi user beamforming scheme for downlink mimo channels based on maximizing signal-to-leakage ratios," in *Proceedings. (ICASSP '05). IEEE International Conference on Acoustics, Speech, and Signal Processing, 2005.*, vol. 3, 2005, pp. iii/1129–iii/1132 Vol. 3.
- [7] H. Weingarten, Y. Steinberg, and S. Shamai, "The capacity region of the gaussian multiple-input multiple-output broadcast channel," *IEEE Transactions on Information Theory*, vol. 52, no. 9, pp. 3936–3964, 2006.
- [8] S. S. Christensen, R. Agarwal, E. De Carvalho, and J. M. Cioffi, "Weighted sum-rate maximization using weighted mmse for mimo-bc beamforming design," *IEEE Transactions on Wireless Communications*, vol. 7, no. 12, pp. 4792–4799, 2008.
- [9] Y. Saito, Y. Kishiyama, A. Benjebbour, T. Nakamura, A. Li, and K. Higuchi, "Non-orthogonal multiple access (noma) for cellular future radio access," in *2013 IEEE 77th Vehicular Technology Conference (VTC Spring)*, 2013, pp. 1–5.

- [10] Y. Mao, O. Dizdar, B. Clerckx, R. Schober, P. Popovski, and H. V. Poor, "Rate-splitting multiple access: Fundamentals, survey, and future research trends," *IEEE Communications Surveys & Tutorials*, vol. 24, no. 4, pp. 2073–2126, 2022.
- [11] S. Chen, B. Ren, Q. Gao, S. Kang, S. Sun, and K. Niu, "Pattern division multiple access—a novel nonorthogonal multiple access for fifth-generation radio networks," *IEEE Transactions on Vehicular Technology*, vol. 66, no. 4, pp. 3185–3196, 2017.
- [12] H. Nikopour and H. Baligh, "Sparse code multiple access," in *2013 IEEE 24th Annual International Symposium on Personal, Indoor, and Mobile Radio Communications (PIMRC)*, 2013, pp. 332–336.
- [13] A. K. Pradhan, V. K. Amalladinne, A. Vem, K. R. Narayanan, and J.-F. Chamberland, "Sparse idma: A joint graph-based coding scheme for unsourced random access," *IEEE Transactions on Communications*, vol. 70, no. 11, pp. 7124–7133, 2022.
- [14] P. Zhang, X. Xu, C. Dong, K. Niu, H. Liang, Z. Liang, X. Qin, M. Sun, H. Chen, and N. Ma, "Model division multiple access for semantic communications," *Frontiers of Information Technology & Electronic Engineering*, vol. 24, no. 6, pp. 801–812, 2023.
- [15] Z. Wu and L. Dai, "Multiple access for near-field communications: Sdma or ldma?" *IEEE Journal on Selected Areas in Communications*, vol. 41, no. 6, pp. 1918–1935, 2023.
- [16] Z. Wu, M. Cui, and L. Dai, "Enabling more users to benefit from near-field communications: From linear to circular array," *IEEE Transactions on Wireless Communications*, vol. 23, no. 4, pp. 3735–3748, 2024.
- [17] P. Antonik, M. Wicks, H. Griffiths, and C. Baker, "Frequency diverse array radars," in *2006 IEEE Conference on Radar*, 2006, pp. 3 pp.–.
- [18] Y. Liao, W.-Q. Wang, and Z. Zheng, "Frequency diverse array beampattern synthesis using symmetrical logarithmic frequency offsets for target indication," *IEEE Transactions on Antennas and Propagation*, vol. 67, no. 5, pp. 3505–3509, 2019.
- [19] Y. Liu, H. Ruan, L. Wang, and A. Nehorai, "The random frequency diverse array: A new antenna structure for uncoupled direction-range indication in active sensing," *IEEE Journal of Selected Topics in Signal Processing*, vol. 11, no. 2, pp. 295–308, 2017.
- [20] Y. Liao, J. Wang, and Q. H. Liu, "Transmit beampattern synthesis for frequency diverse array with particle swarm frequency offset optimization," *IEEE Transactions on Antennas and Propagation*, vol. 69, no. 2, pp. 892–901, 2021.
- [21] A.-M. Yao, W. Wu, and D.-G. Fang, "Frequency diverse array antenna using time-modulated optimized frequency offset to obtain time-invariant spatial fine focusing beampattern," *IEEE Transactions on Antennas and Propagation*, vol. 64, no. 10, pp. 4434–4446, 2016.
- [22] S. Han, C. Fan, and X. Huang, "Frequency diverse array with time-dependent transmit weights," in *2016 IEEE 13th International Conference on Signal Processing (ICSP)*, 2016, pp. 448–451.
- [23] Y. Liao, G. Zeng, Z. Luo, and Q. H. Liu, "Time-variance analysis for frequency-diverse array beampatterns," *IEEE Transactions on Antennas and Propagation*, vol. 71, no. 8, pp. 6558–6567, 2023.
- [24] Y. Xu and K.-M. Luk, "Enhanced transmit–receive beamforming for frequency diverse array," *IEEE Transactions on Antennas and Propagation*, vol. 68, no. 7, pp. 5344–5352, 2020.
- [25] A. Basit, W.-Q. Wang, S. Y. Nusenu, and S. Zhang, "Range-angle-dependent beampattern synthesis with null depth control for joint radar communication," *IEEE Antennas and Wireless Propagation Letters*, vol. 18, no. 9, pp. 1741–1745, 2019.
- [26] M. Li and W.-Q. Wang, "Joint radar-communication system design based on fda-mimo via frequency index modulation," *IEEE Access*, vol. 11, pp. 67 722–67 736, 2023.

- [27] J. Jian, Q. Huang, B. Huang, and W.-Q. Wang, "Fda-mimo-based integrated sensing and communication system with frequency offset permutation index modulation," *arXiv preprint arXiv:2312.14468*, 2023.
- [28] J. Jian, W.-Q. Wang, B. Huang, L. Zhang, M. A. Imran, and Q. Huang, "Mimo-fda communications with frequency offsets index modulation," *IEEE Transactions on Wireless Communications*, vol. 23, no. 5, pp. 4580–4595, 2024.
- [29] A. Basit, W.-Q. Wang, S. Y. Nusenu, and S. Wali, "Fda based qsm for mmwave wireless communications: Frequency diverse transmitter and reduced complexity receiver," *IEEE Transactions on Wireless Communications*, vol. 20, no. 7, pp. 4571–4584, 2021.
- [30] J. Jian, W.-Q. Wang, H. Chen, and B. Huang, "Physical-layer security for multi-user communications with frequency diverse array-based directional modulation," *IEEE Transactions on Vehicular Technology*, vol. 72, no. 8, pp. 10 133–10 145, 2023.
- [31] D. Tse and P. Viswanath, *Fundamentals of Wireless Communication*. Cambridge University Press, 2005.
- [32] J. Li, H. Li, and S. Ouyang, "Identifying unambiguous frequency pattern for target localization using frequency diverse array," *Electronics Letters*, vol. 53, no. 19, pp. 1331–1333, 2017.
- [33] P. Patcharamaneepakorn, S. Armour, and A. Doufexi, "On the equivalence between slnr and mmse precoding schemes with single-antenna receivers," *IEEE Communications Letters*, vol. 16, no. 7, pp. 1034–1037, 2012.
- [34] Y.-G. Lim, C.-B. Chae, and G. Caire, "Performance analysis of massive mimo for cell-boundary users," *IEEE Transactions on Wireless Communications*, vol. 14, no. 12, pp. 6827–6842, 2015.
- [35] K.-K. Wong and Z. Pan, "Array gain and diversity order of multiuser miso antenna systems," *International Journal of Wireless Information Networks*, vol. 15, pp. 82–89, 2008.